

We now examine the probability (or frequency) distribution of meteorological predictions and the measurements. Figure 12 presents the observed and model probability (expressed as probability density function (pdf)) of occurrence of a particular value of (a) wind speed, (b) wind direction, (c) temperature, (d) net radiation and (e) relative humidity at Bancell Road. The values of a given meteorological variable were binned and the number of values in a particular bin were normalised by the total number of values to obtain the probability. The bin size for a given variable was constant and is equal to the separation between two successive points in Figure 12. The data point is plotted for the upper value of the range, e.g. 3 m s^{-1} for the $2\text{--}3 \text{ m s}^{-1}$. For example, the bin size in Figure 12a is 1 m s^{-1} , and a probability of 0.15 at 3 m s^{-1} in the data curve means that 15% of the data are greater than 2 m s^{-1} and less than or equal to 3 m s^{-1} . The model is able to reproduce the observed pdf for wind speed reasonably well (Figure 12a), with the probabilities corresponding to both model and observed peaks almost the same, but with the wind speeds corresponding to these peaks separated by about 1.5 m s^{-1} . It is also clear that for wind speeds less than 5 m s^{-1} the model predictions are less frequent than the observations, and vice versa for winds speed higher than 5 m s^{-1} .

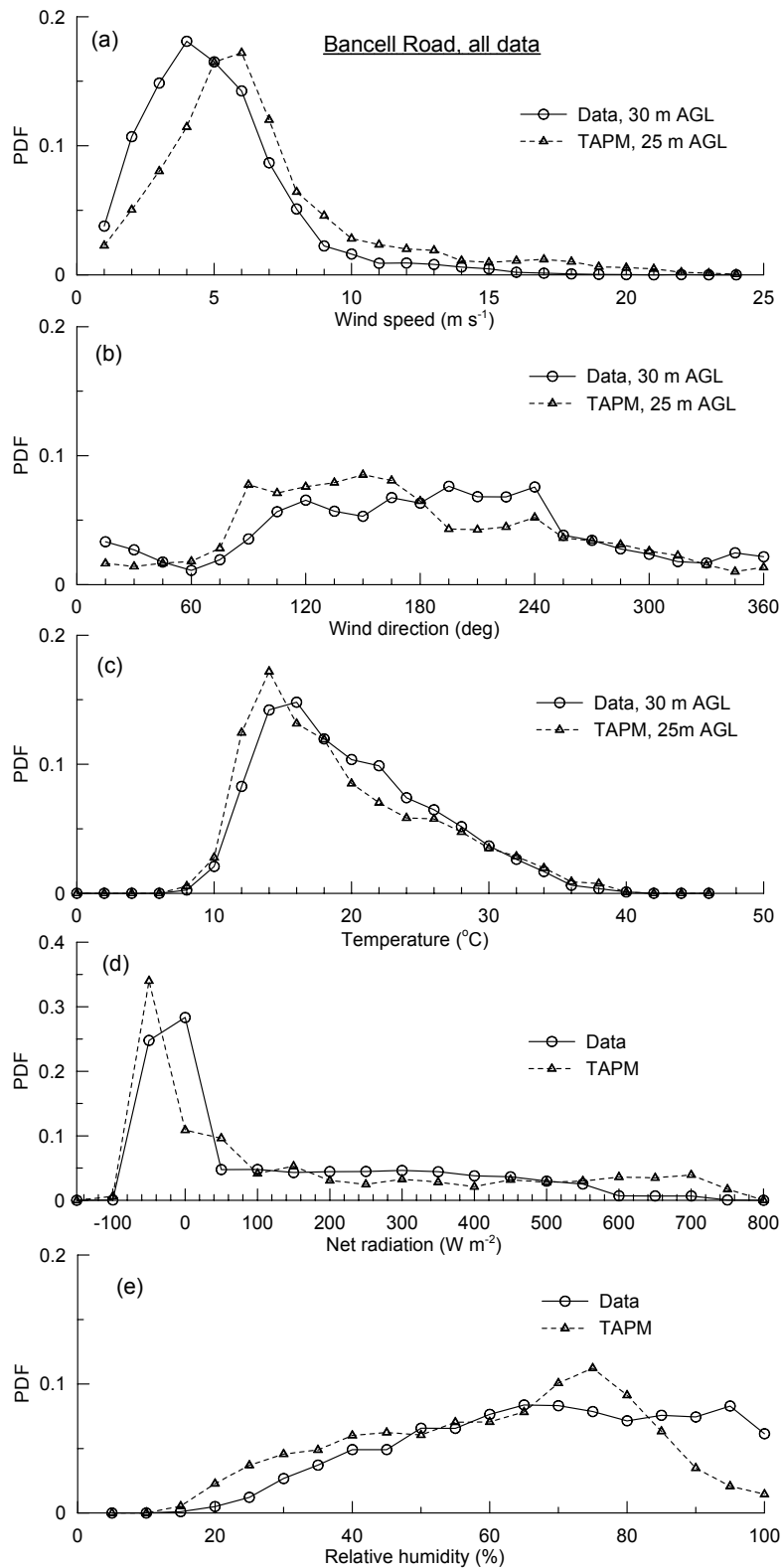


Figure 12: The observed and model probability (expressed as probability density function (pdf)) of occurrence of parameter values for (a) wind speed, (b) wind direction, (c) temperature, (d) net radiation, and (e) relative humidity at Bancell Road. The net radiation and relative humidity are measured at about 1 m AGL while the other parameters are measured at 30 m AGL.

In Figure 12b, the winds from the south-east quadrant predicted by the model are more frequent than the observations, and vice versa for the winds from the south-west quadrant. The northerly winds are predicted less frequently by the model (see Section 6.8 for a detailed comparison). The temperature frequencies are predicted very well by the model (Figure 12c). The model and observed net radiation plots (Figure 12d) are qualitatively similar, with the model showing a somewhat narrower peak, and higher frequencies for extreme values than the data. For the relative humidity values greater than 80%, the model frequency is smaller than the data (Figure 12e).

Table 6 gives the model evaluation statistics for wind speed (WS) ($m\ s^{-1}$), the west-east component (U) of the horizontal wind vector ($m\ s^{-1}$), the south-north component (V) of the horizontal wind vector ($m\ s^{-1}$), ambient temperature (T) ($^{\circ}C$), net radiation (R_n) ($W\ m^{-2}$), and relative humidity (R_H) (%) calculated using all data. We cannot use the wind direction values directly for calculating evaluation statistics due to the discontinuity at north, and therefore, the wind components are used instead. A positive V indicates a southerly wind component, whereas a negative V indicates a northerly wind component. Similarly, a positive U indicates a westerly wind component, whereas a negative U indicates an easterly wind component. Table 6 shows that TAPM predicts a stronger mean wind than the measurements. The model has a tendency to predict slightly stronger mean south-north component (V) of the wind vector. On the other hand, the model mean U component of the wind vector is much stronger than the observed value, indicating that the model is predicting stronger and/or more frequent easterly winds than the data suggest. The signs of the U and V components are the same for the measurements and the model results, which suggest that overall the dominant model winds (in terms of *both* strength and frequency) are from the same quadrant (south-east) as the observed ones. The correlation coefficient (r) for the wind components is better than that for wind speed, suggesting that the model wind directions are generally better correlated with the data than wind speeds. For all variables, $RMSE_S$ is smaller than $RMSE_U$, which, as mentioned earlier, is a characteristic of a good model. The predicted standard deviations (P_{std}) are larger than the observed values (O_{std}) for all parameters, except relative humidity. The index of agreement (IOA) is the highest for temperature, followed by net radiation, V -component, relative humidity, U -component, and wind speed.

Table 6: Model evaluation statistics for Bancell Road at 30 m AGL, all data

Variable	N	O_{mean}	P_{mean}	O_{std}	P_{std}	r	$RMSE$	$RMSE_S$	$RMSE_U$	IOA
WS	5585	4.5	6.3	2.6	3.9	0.51	3.85	1.94	2.25	0.65
U	5585	-0.4	-2.3	4.0	5.9	0.73	4.47	1.95	4.02	0.79
V	5585	1.3	1.8	3.1	3.3	0.85	1.81	0.52	1.74	0.92
T	5806	18.8	18.3	6.0	6.5	0.95	2.01	0.69	1.24	0.97
R_n	5774	101.6	143.3	193.2	257.4	0.93	111.97	34.79	71.38	0.94
R_H	8380	65.8	58.3	20.3	20.1	0.82	14.22	9.52	10.75	0.87

KEY: N = Number of observations, O = Observations, P = Model Predictions, $mean$ = Arithmetic mean, std = Standard Deviation, r = Correlation Coefficient (0 = no correlation, 1 = perfect positive correlation, -1 = perfect negative correlation), $RMSE$ = Root

Mean Square Error, $RMSE_S$ = Systematic Root Mean Square Error, $RMSE_U$ = Unsystematic Root Mean Square Error, IOA = Index of Agreement (0 = no agreement, 1 = perfect agreement).

6.4.2 Daytime (0800–1900 h)

It is instructive to perform separate analyses for daytime (0800–1900 h) and nighttime (2000–0700 h) in order to examine if there are any prominent differences between the model results and the data for the two parts of a diurnal cycle. Generally, in the nighttime, the flow is sensitive to local topographical and land-use characteristics, and can be quite different from regional flow patterns. On the other hand, in the daytime, the atmospheric mixing generated by the upward surface heat flux leads to a more spatially uniform flow than in the nighttime. It can, therefore, be anticipated that a meteorological model would generally do better in the daytime than in the nighttime.

Figure 13 shows scatter plots of model predictions vs. observed data for wind speed, wind direction, temperature, net radiation, and relative humidity at Bancell Road for the daytime hours. A qualitative comparison of Figure 13a with Figure 10a, and of Figure 13b with Figure 10b suggests that for wind predictions the model is performing a lot better for the daytime than for all hours (implying that the differences between the model winds and the data may be large in the nighttime, see Section 6.4.3). The temperature, net radiation and relative humidity scatter plots are similar to those in Figure 10.

Bancell Road, daytime, 30 m

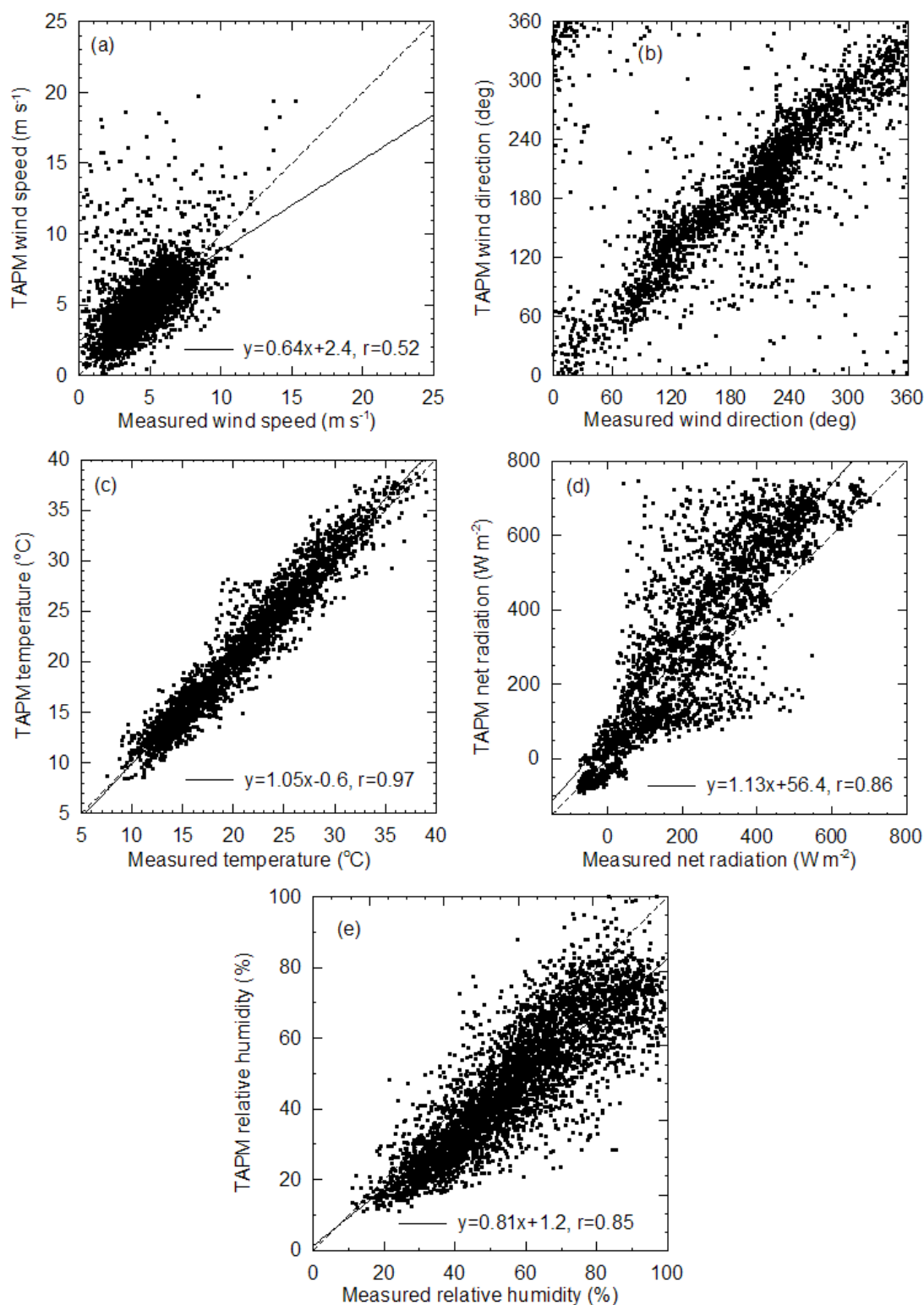


Figure 13: Scatter plots of model predictions vs. observed data for the daytime hours (0800–1900 h) for (a) wind speed, (b) wind direction, (c) temperature, (d) net radiation, and (e) relative humidity at Bancell Road. The net radiation and relative humidity are measured at about 1 m AGL, while the other parameters are measured at 30 m AGL.

Figure 14 presents the probability (or frequency) distributions of the model predictions and the measurements for daytime. The model frequency distribution of wind speed matches well with the observed distribution (Figure 14a). TAPM predicts a higher frequency of the southerly winds and lower frequency of the south-westerly winds, but the rest of the model distribution is reasonably close to the observations (Figure 14b). The agreement between the model temperature distribution and the observed temperature distribution is very good (Figure 14c), with the model able to predict the double peaks as seen in the data curve. The model predicts a higher frequency of net radiation for the extreme end of the distribution (Figure 14d). The model and the observed relative humidity frequency plots match reasonably well, with both showing a peak at around 60%; however, the model underpredicts high relative humidity ($\geq 80\%$) and overpredicts low relative humidity ($\leq 40\%$) compared with the observations (Figure 14e).

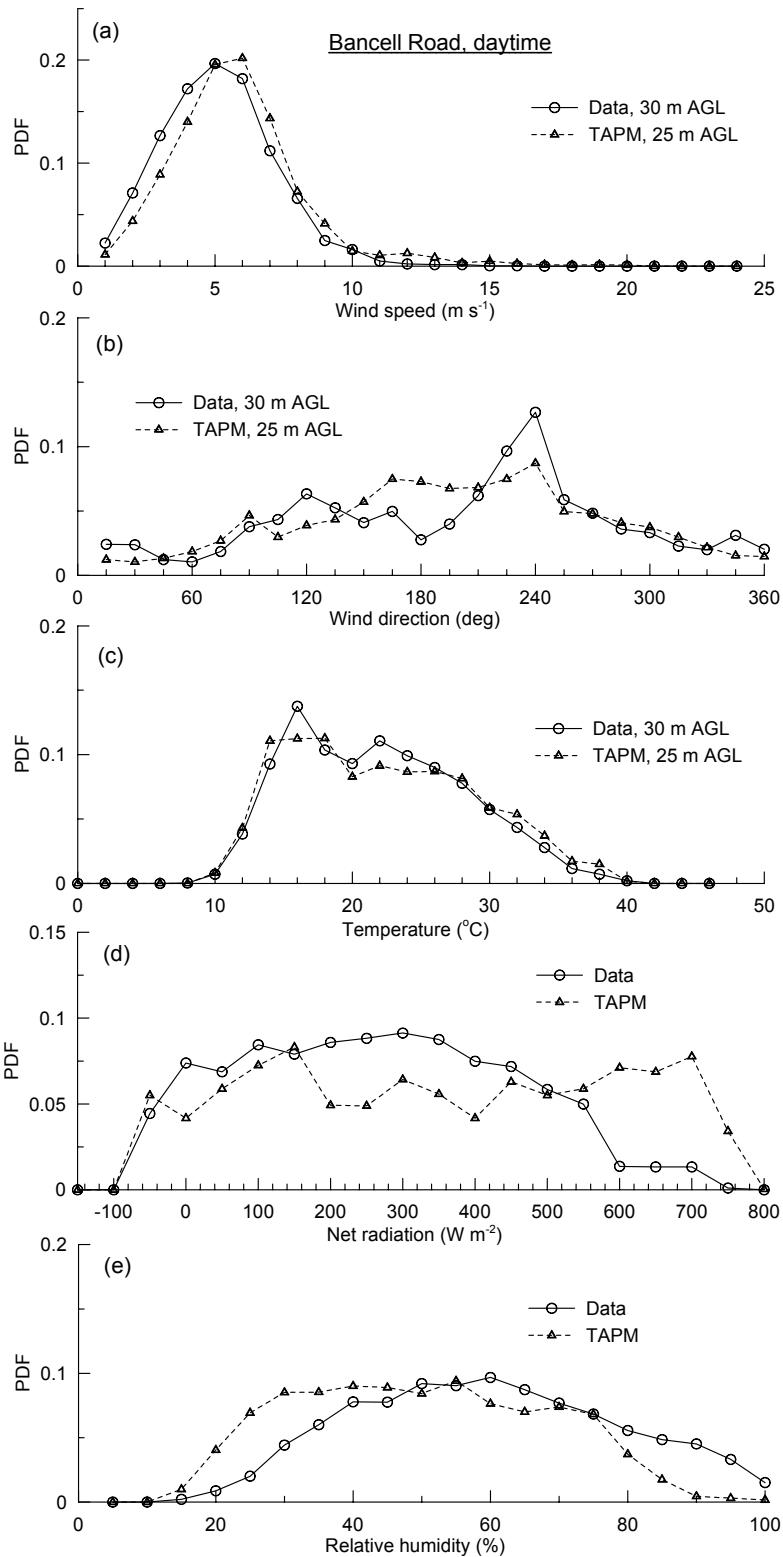


Figure 14: The observed and model probability (expressed as probability density function (pdf) of occurrence of parameter values for daytime (0800–1900 h) for (a) wind speed, (b) wind direction, (c) temperature, (d) net radiation, and (e) relative humidity at Bancell Road. The net radiation and relative humidity are measured at about 1 m AGL while the other parameters are measured at 30 m AGL.

Overall, the model evaluation statistics in Table 7 for daytime are certainly better than those in Table 6, although the model is still predicting slightly stronger wind speeds. The temperature is very well predicted by the model. The model mean net radiation is larger by about 100 W m^{-2} . For relative humidity, the $RMSE_S$ value is slightly greater than the $RMSE_U$ value.

Table 7: Model evaluation statistics for Bancell Road at 30 m AGL, daytime

Variable	N	O_{mean}	P_{mean}	O_{std}	P_{std}	r	$RMSE$	$RMSE_S$	$RMSE_U$	IOA
WS	2858	4.6	5.4	2.0	2.5	0.52	2.36	1.10	2.13	0.70
U	2858	0.6	0.1	3.7	4.4	0.79	2.77	0.53	2.72	0.87
V	2858	1.2	1.8	3.2	3.5	0.87	1.80	0.59	1.70	0.92
T	2944	20.9	21.3	6.2	6.7	0.97	1.77	0.11	1.25	0.98
R_n	2924	239.9	328.3	184.4	242.9	0.86	154.13	70.40	99.80	0.87
R_H	4227	57.1	47.5	19.0	18.0	0.85	13.90	11.95	10.50	0.86

6.4.3 Nighttime (2000–0700 h)

Figure 15 shows scatter plots of the model meteorological predictions vs. the observations at Bancell Road for the nighttime hours. The model calculates much stronger winds than the measurements in the nighttime (Figure 15a). Much of the differences between the model winds and the measurements in the comparison for all hours (Figure 10a and Figure 10b) are dominated by the differences in the nighttime. Both the model results and the measurements indicate that the strongest of the nighttime winds are generally dominated by the easterlies, and that, overall, the nighttime winds are stronger than the daytime values. The nighttime temperatures are predicted well by TAPM, although there is a tendency in the model to estimate slightly lower temperatures in the high range (Figure 15c). Some of the high values of net radiation are overestimated by TAPM (Figure 15d), although the correlation coefficient is relatively high at 0.8. The relative humidity comparison in Figure 15e, with a correlation coefficient of 0.68, is not as good as that in the daytime.

Bancell Road, nighttime, 30 m

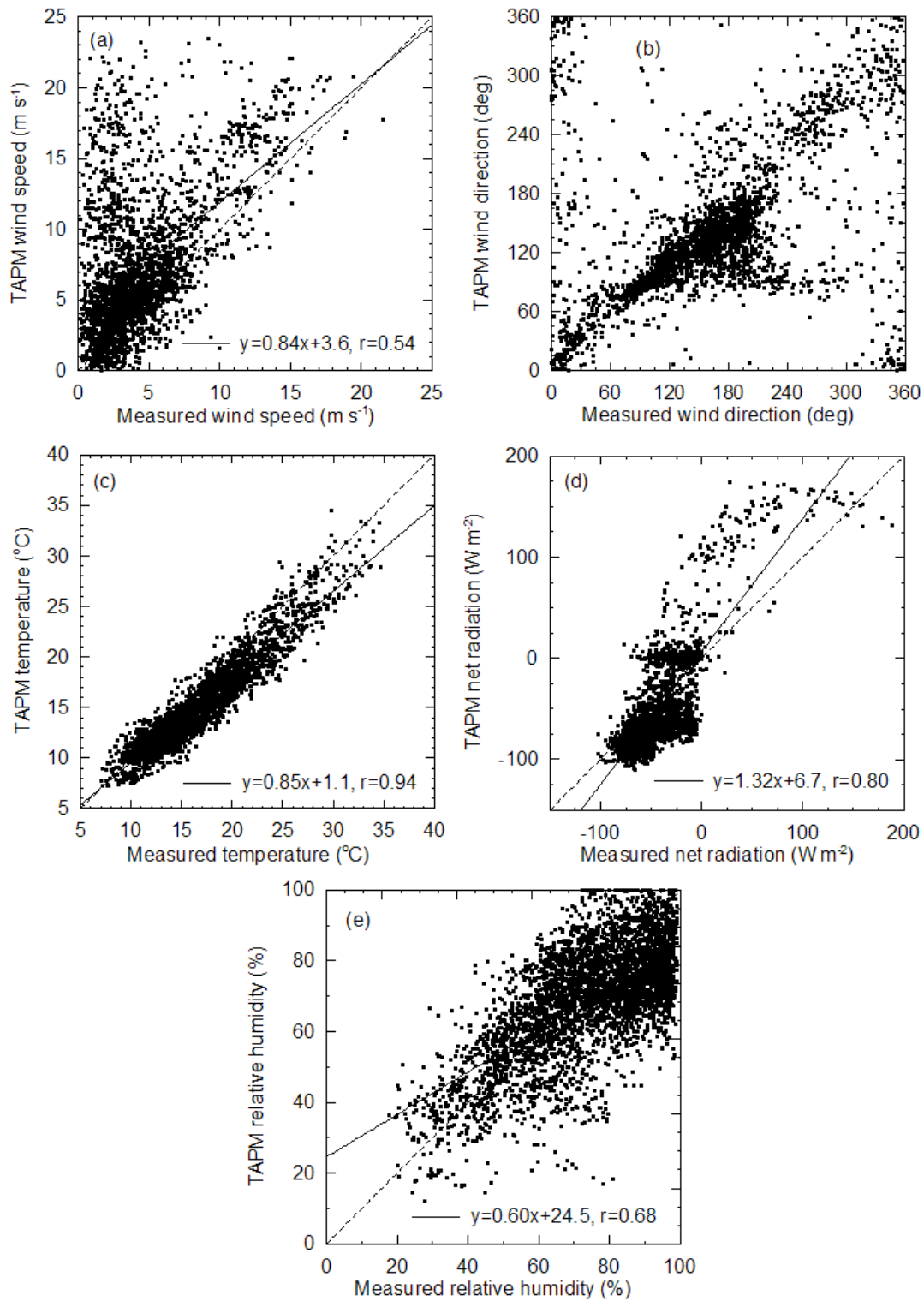


Figure 15: Scatter plots of model predictions vs. observed data for the nighttime hours (2000–0700 h) for (a) wind speed, (b) wind direction, (c) temperature, (d) net radiation, and (e) relative humidity at Bancell Road. The net radiation and relative humidity are measured at about 1 m AGL, while the other parameters are measured at 30 m AGL.

Figure 16a shows that compared to the data, TAPM predicts less frequent wind speeds below 5 m s^{-1} and more frequent wind speeds above this value. The most frequent model winds are from the south-east sector, whereas the data curve shows southerlies to be the most frequent (Figure 16b). The model has a slight tendency to predict more frequent temperature events below 15°C and less frequent temperature events above this value (Figure 16c). The net radiation agreement in Figure 16d looks satisfactory. The highest frequency predicted by TAPM for relative humidity is for the value of 75%, whereas the corresponding observed value is 95% (Figure 16e). For the relative humidity values less than 65%, both the model and observed curves match closely.

TAPM performance can be tested when the model predictions of the strong easterly flow (between 45° – 135°) are excluded from the comparison analysis. Figure 17a shows the probability distributions of wind-speed values for nighttime without the model easterlies, whereas Figure 17b presents the corresponding scatter plot. A comparison of Figure 17a with Figure 16a indicates that the exclusion of the model easterlies leads to an overall improvement in the model frequency distribution, although the tendency of TAPM to predicts less frequent wind speeds below about 5 m s^{-1} remains (but is reduced). This becomes even clearer when Figure 17b is compared with Figure 16b; the correlation coefficient in the former is 0.64 while in the latter it is 0.54.

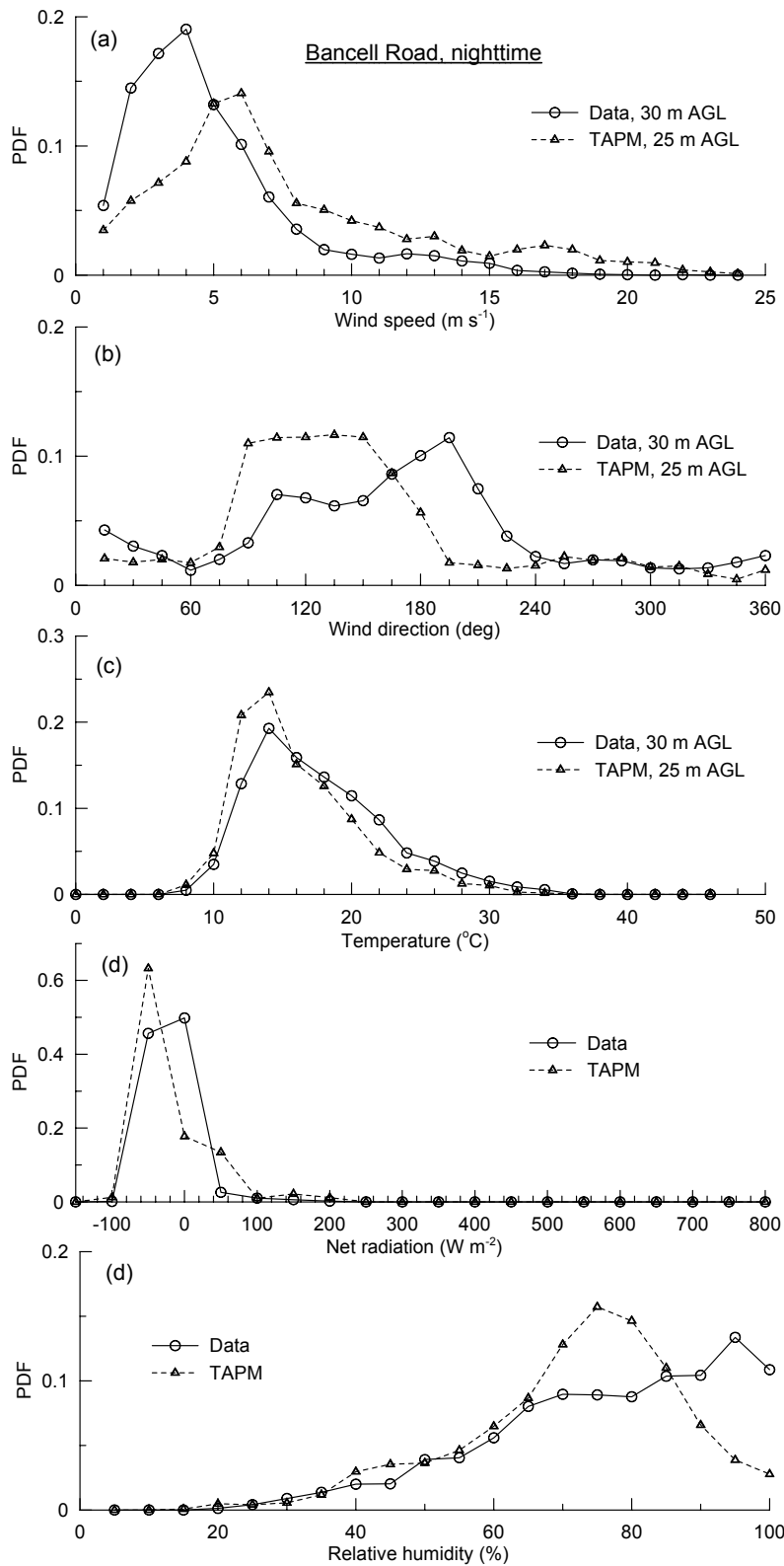


Figure 16: The observed and model probability (expressed as probability density function (pdf) of occurrence of parameter values for nighttime (2000–0700 h) for (a) wind speed, (b) wind direction, (c) temperature, (d) net radiation, and (e) relative humidity at Bancell Road. The net radiation and relative humidity are measured at about 1 m AGL while the other parameters are measured at 30 m AGL.

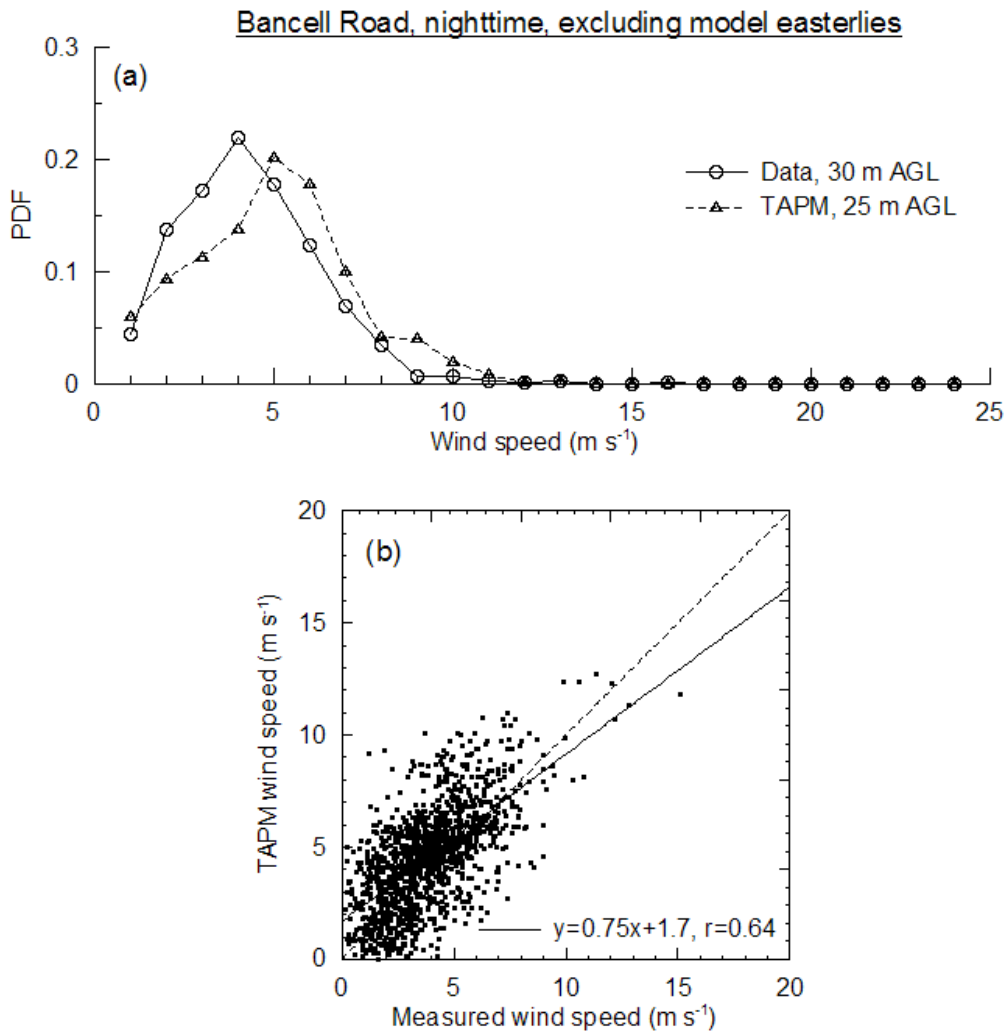


Figure 17: (a) the observed and model probability (expressed as probability density function (pdf) of occurrence of wind speed values for nighttime (2000–0700 h) at Bancell Road when hours during which the model wind directions are between 45°–135° (easterlies) are excluded from the analysis; (b) the corresponding scatter plot of model predictions vs. observed.

Table 8 for nighttime indicates that the model has a much stronger easterly component than the data (also apparent in Figure 16a). The mean net radiation is predicted well. Overall, the values of correlation coefficient and IOA are satisfactory to very good. Both model and observations indicate that mean nighttime relative humidity values are larger than those in the daytime, and that the predictions are somewhat better in the daytime than in the nighttime.

Table 8: Model evaluation statistics for Bancell Road at 30 m AGL, nighttime

Variable	N	O_{mean}	P_{mean}	O_{std}	P_{std}	r	$RMSE$	$RMSE_S$	$RMSE_U$	IOA
WS	2727	4.4	7.3	3.1	4.8	0.54	4.95	2.95	2.74	0.64
U	2727	-1.5	-4.9	4.1	6.2	0.66	5.74	3.41	4.61	0.70
V	2727	1.4	1.8	2.9	3.2	0.83	1.83	0.47	1.77	0.91
T	2862	16.6	15.2	5.0	4.5	0.94	2.23	0.94	1.09	0.94
R_n	2850	-40.4	-46.5	30.8	50.4	0.80	32.05	5.93	36.53	0.84
R_H	4153	74.6	69.2	17.7	15.6	0.68	14.54	10.15	10.87	0.80

6.4.4 Winter period (1 April–30 September 2003) including low to moderate wind speeds ($\leq 3 \text{ m s}^{-1}$)

Scatter plots of the model predictions vs. the observations for the period 1 April–30 September 2003, which includes the winter months, are presented in Figure 18. Note that the temperature and wind measurements at 30 m AGL only started from 18 July 2003. The temperature, net radiation and relative humidity are better predicted than the wind speed. It is observed that the winds are better predicted for wintertime whereas the temperature, net radiation and relative humidity are somewhat better predicted for summertime (see next Section).

For the winter period, TAPM is predicting a lower frequency of wind speeds less than 4 m s^{-1} compared to the observations (Figure 19a). TAPM predicts winds between 0–1, 1–2 and 2–3 m s^{-1} for 3.6%, 9.1% and 14.0% of the time, respectively, whereas the corresponding observed frequencies are 6.5%, 16.3% and 19.7%. The predicted frequency of northerly surface winds is smaller than the measurements (Figure 19b), whereas the temperature frequencies are very well predicted by the model (Figure 19c). The model net radiation curve shows a double-peak variation as opposed to the observed single peak curve (Figure 19d). The maximum observed frequency of relative humidity is for a value of about 95%, which can be contrasted with the corresponding model value of 75% (Figure 19e).

Bancell Road, winter, 30 m

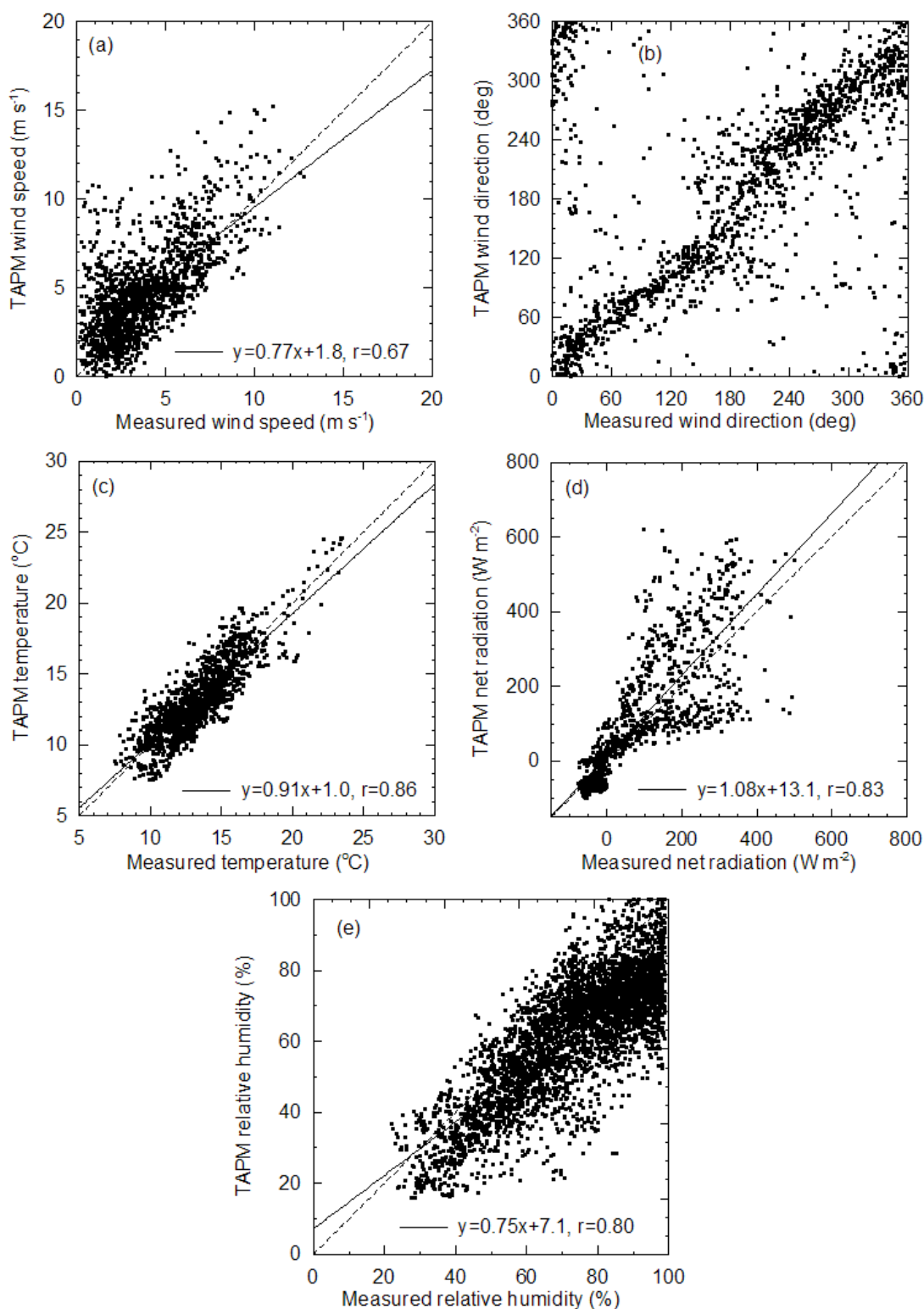


Figure 18: Scatter plots of model predictions vs. observed data for the winter months for (a) wind speed, (b) wind direction, (c) temperature, (d) net radiation, and (e) relative humidity at Bancell Road. The net radiation and relative humidity are measured at about 1 m AGL, while the other parameters are measured at 30 m AGL.

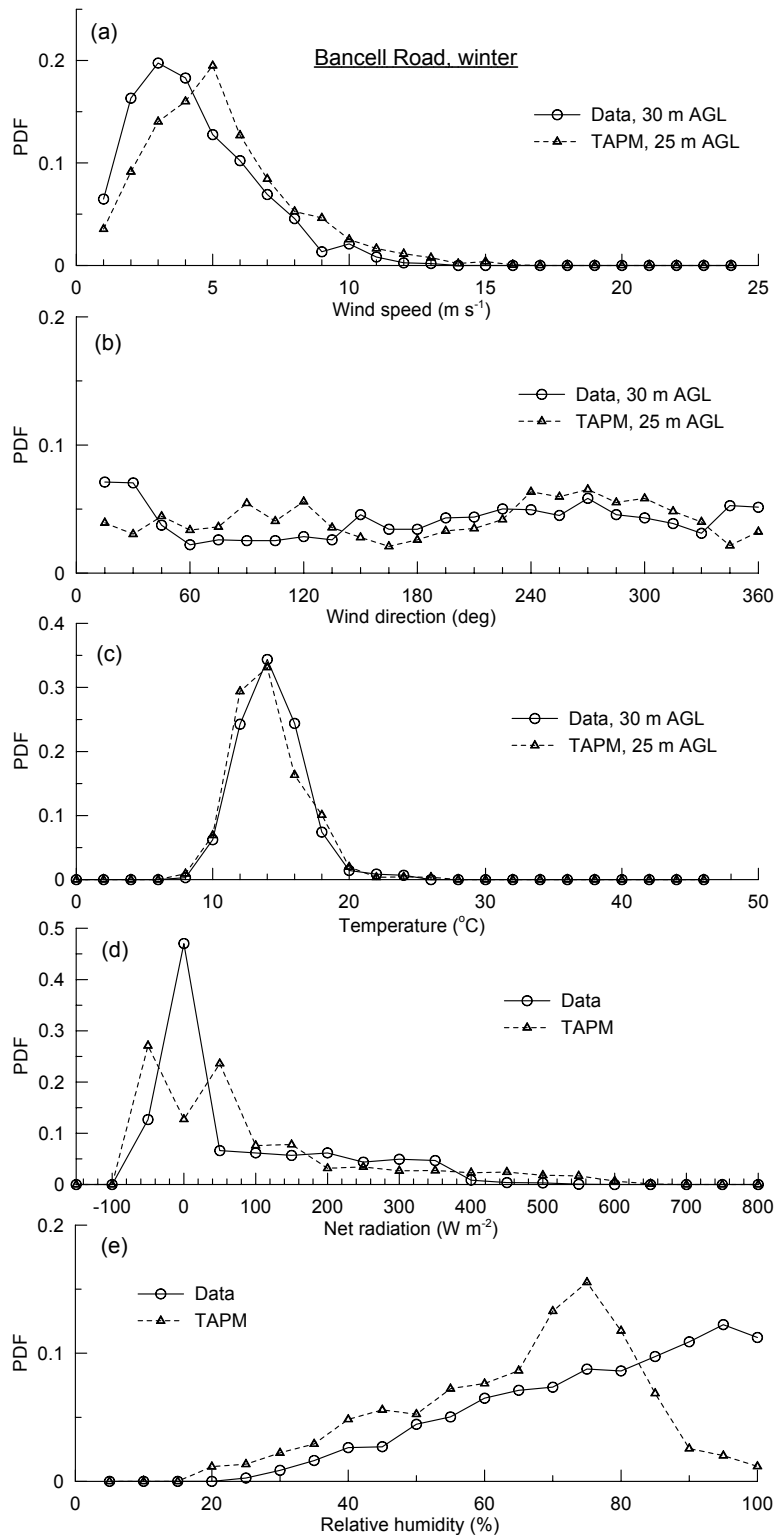


Figure 19: The observed and model probability (expressed as probability density function (pdf) of occurrence of parameter values for the winter months for (a) wind speed, (b) wind direction, (c) temperature, (d) net radiation, and (e) relative humidity at Bancell Road. The net radiation and relative humidity are measured at about 1 m AGL while the other parameters are measured at 30 m AGL.

The model evaluation statistics for the wintertime are given in Table 9. The signs of the U and V components suggest that the dominant model winds are from the same quadrant (north-west) as the observed ones.

Table 9: Model evaluation statistics for Bancell Road at 30 m AGL, winter

Variable	N	O_{mean}	P_{mean}	O_{std}	P_{std}	r	$RMSE$	$RMSE_S$	$RMSE_U$	IOA
WS	1575	3.8	4.8	2.2	2.6	0.67	2.19	1.04	1.98	0.79
U	1575	0.6	0.3	3.0	4.3	0.80	2.59	0.52	2.54	0.86
V	1575	-0.6	-0.4	3.1	3.3	0.88	1.63	0.33	1.60	0.93
T	1603	13.3	13.1	2.4	2.5	0.86	1.33	0.26	1.19	0.92
R_n	1601	50.5	67.8	122.1	158.3	0.83	89.39	17.90	64.79	0.89
R_H	4177	73.8	62.6	18.2	17.1	0.80	15.77	11.84	10.53	0.81

6.4.5 Summer period (1 October 2003–31 March 2004)

Scatter plots of the modelled meteorology vs. the observations for the period 1 October 2003–31 March 2004 are shown in Figure 20. As mentioned earlier, the winds are better predicted in the winter period, whereas the temperature, net radiation and relative humidity better predicted in the summer period. In Figure 20, the temperature, net radiation and relative humidity are better predicted than the wind speed.

For the summer period, the observed frequency of wind speeds greater than 10 m s^{-1} (Figure 21a) is slightly higher in the summer than in the winter (Figure 18a), a behaviour also shown by the model frequency curves. The most frequent observed wind direction sector is 90° – 240° , which is also suggested by the model, but the model southeasterly winds are more frequent than the observations. The temperature frequencies are reasonably well predicted by the model (Figure 21b). The model performance is good in describing the net radiation and relative humidity probabilities. Both the model and observed curves show smaller frequencies of high humidity values in the summer period than in the winter period.

The model evaluation statistics for the summer period given in Table 10 indicates that the model easterly wind component is much higher than the observed value. The best IOA is for temperature, followed by net radiation, relative humidity, and the winds (this is almost always the case for any site, due in part to the difference between variables).

Bancell Road, summer, 30 m

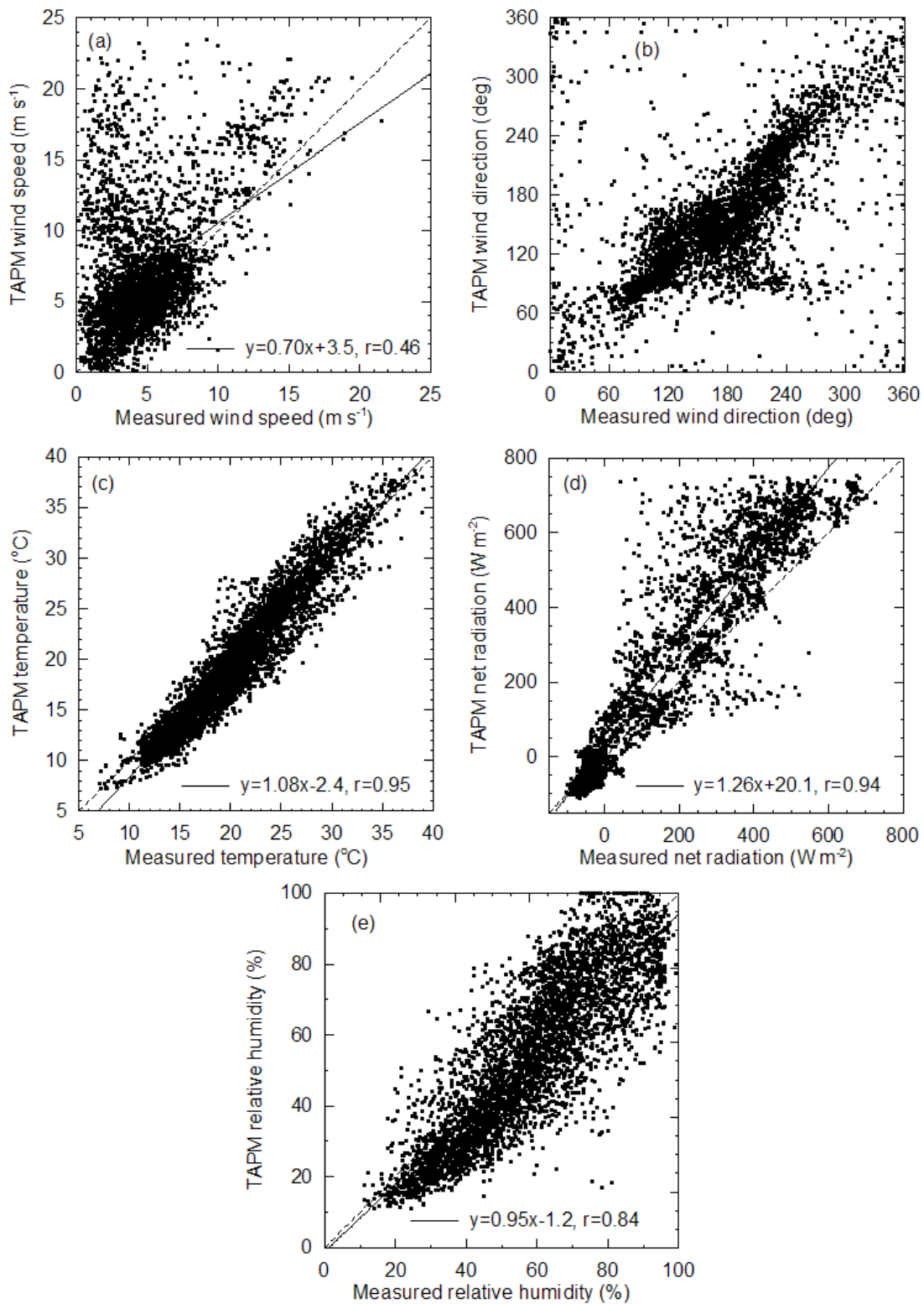


Figure 20: Scatter plots of model predictions vs. observed data for the summer months for (a) wind speed, (b) wind direction, (c) temperature, (d) net radiation, and (e) relative humidity at Bancell Road. The net radiation and relative humidity are measured at about 1 m AGL, while the other parameters are measured at 30 m AGL.

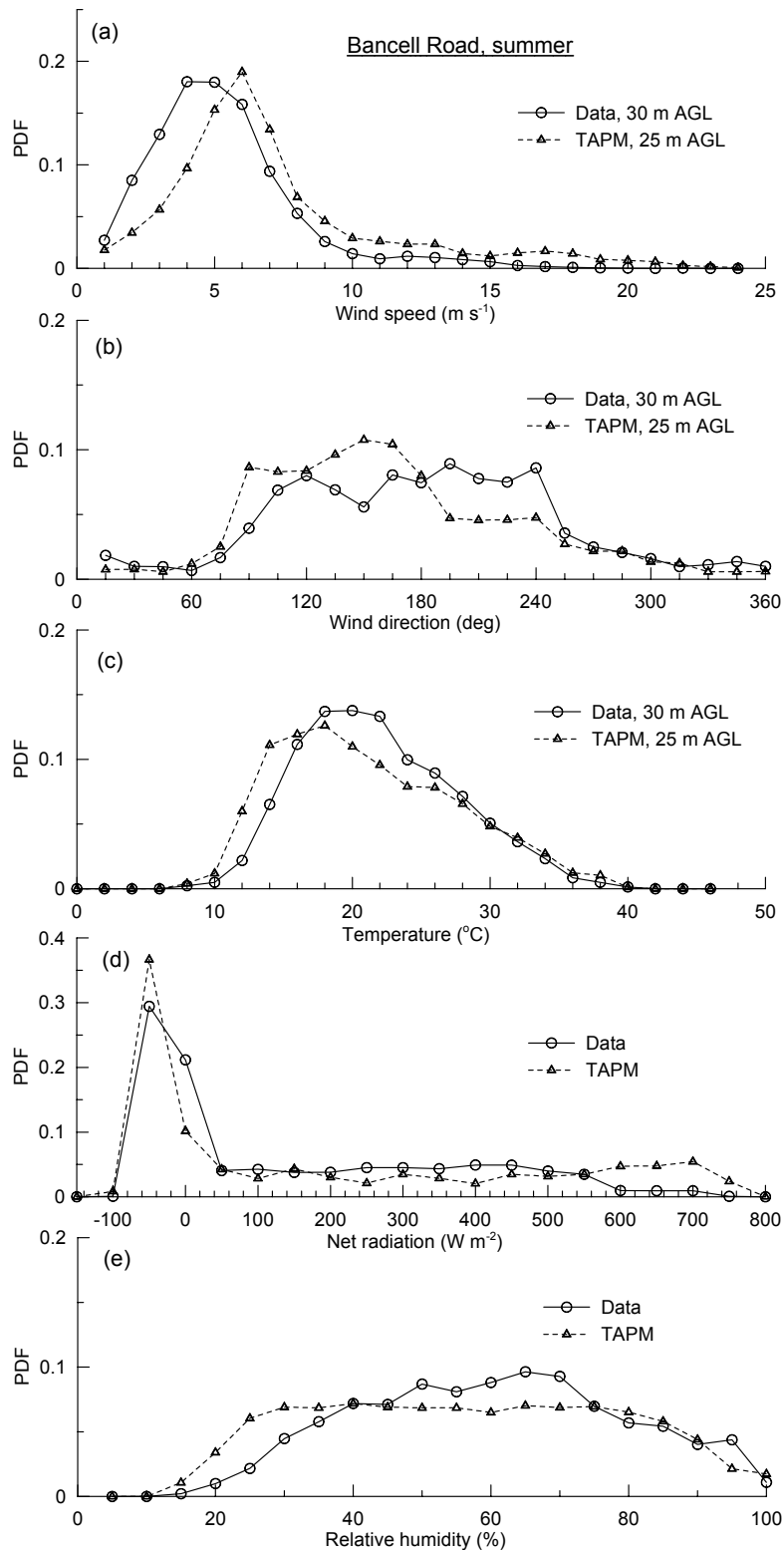


Figure 21: The observed and model probability (expressed as probability density function (pdf) of occurrence of parameter values for the summer months for (a) wind speed, (b) wind direction, (c) temperature, (d) net radiation, and (e) relative humidity at Bancell Road. The net radiation and relative humidity are measured at about 1 m AGL while the other parameters are measured at 30 m AGL.

Table 10: Model evaluation statistics for Bancell Road at 30 m AGL, summer

Variable	N	O_{mean}	P_{mean}	O_{std}	P_{std}	r	$RMSE$	$RMSE_S$	$RMSE_U$	IOA
WS	4010	4.8	6.9	2.7	4.2	0.46	4.33	2.21	3.82	0.61
U	4010	-0.8	-3.4	4.3	6.2	0.71	5.02	2.56	4.32	0.76
V	4010	2.1	2.7	2.7	2.9	0.80	1.88	0.65	1.77	0.88
T	4203	20.9	20.3	5.6	6.5	0.95	2.21	0.87	1.99	0.97
R_n	4173	121.2	172.3	211.1	281.1	0.94	119.50	77.81	100.10	0.94
R_H	4203	57.9	53.9	19.2	21.8	0.84	12.49	4.12	11.83	0.90

6.5. Model evaluation with the Wagerup-specific land-use and Refinery heat-flux configuration – Bancell Road (10 m)

Wind speed, wind direction and temperature modelled at a height of 10 m were calculated with the intention that they be compared with the corresponding observations at 10 m AGL at Bancell Road. Figure 22 shows the observed and model variations of wind speed with wind direction at 10 m AGL at Bancell Road. It is apparent that the strong easterly winds predicted by the model are almost nonexistent in the observations. The main reason for this is the fact that the 10-m wind sensor is sheltered from due easterly winds by the (solid) mast and is only about one and a half mast width away from the mast (see Figure 23).

The SKM (2003) audit report on the meteorological observations states that the 10-m wind sensor does not meet the Australian Class 1 station standard, partly because of the sheltering of the sensor, but the 30-m sensor meets the exposure standards.

Because of the above issues concerning the reliability of the 10-m wind observations, a full comparison of the model results with the 10-m observations would not be done and presented. To minimise the influence of sheltering by the mast in the data analysis, we removed all hours for which the observed 10-m wind direction was within the sector $45^\circ - 145^\circ$ (the sector is slightly skewed towards south-east because the boom connecting to the solid mast is attached to the northern face of the mast), and used the filtered wind data for model comparison. No filtering was applied to the 10-m temperature data. Even with this filtering, the rest of the 10-m wind data may still carry some influence of the mast. The Australian Standard AS 2923 (1987) “Guide for Measurement of Horizontal Wind for Air Quality Applications” (for rotating cup and propeller type anemometers) refers to an article by Gill et al. (1967) which says that using a boom extension of $3D$ ($D =$ tower diameter) on stacks (i.e. circular solid towers) one can obtain wind speed measurements accurate to within $\pm 10\%$ of true value through an arc of about 180° , and wind direction measurements true within $\pm 5\%$ for an arc of about 300° . (If winds accurate within $\pm 10\%$ in speed and $\pm 5^\circ$ in direction are needed for the complete 360° of azimuth, two sets of speed and direction sensors, 180° apart and located not less than $3D$ out from the solid tower, are recommended.)

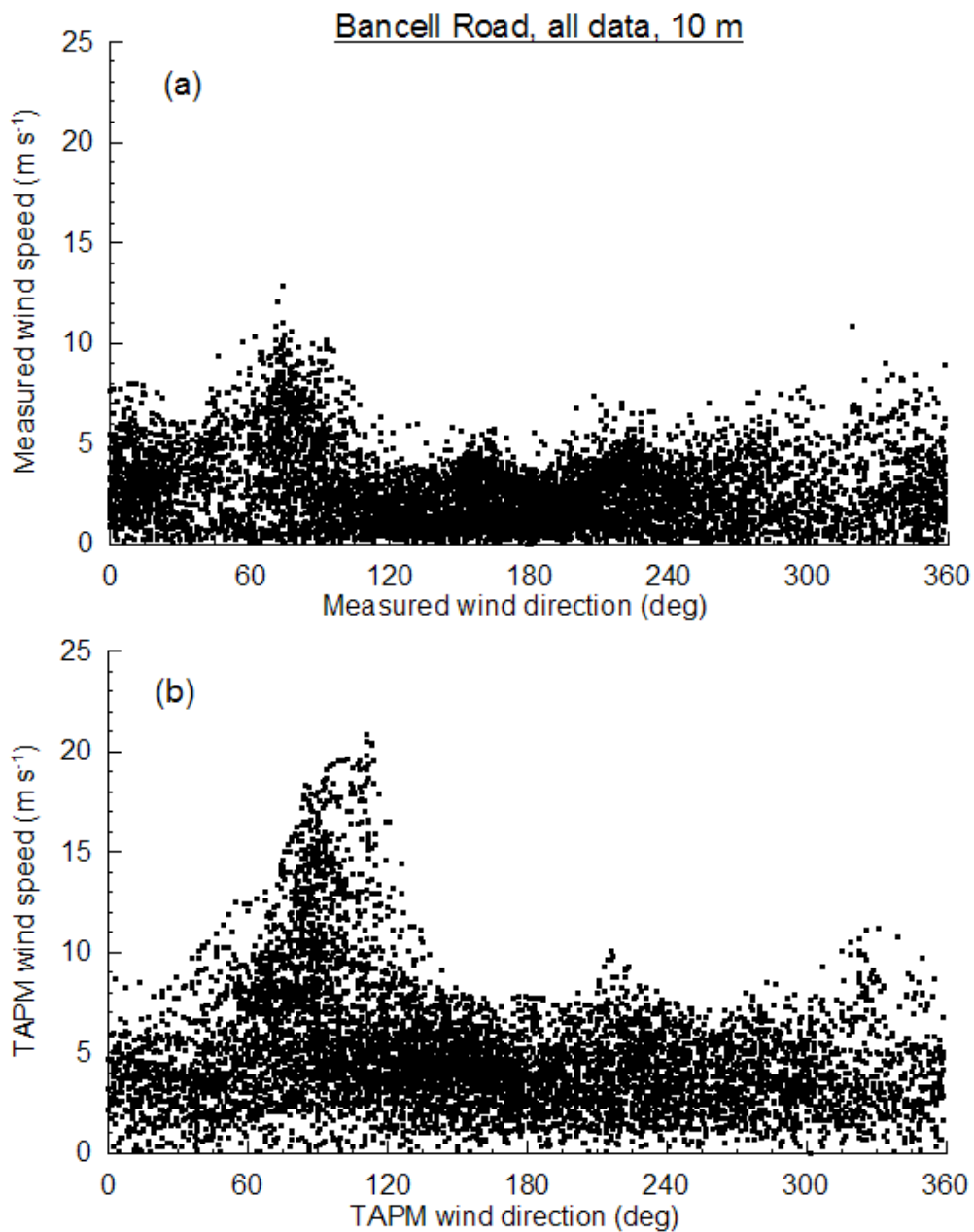


Figure 22: Variation of wind speed with wind direction at 10 m AGL at Bancell Road: (a) observations and (b) model predictions.



Figure 23: 10-m wind sensor at Bancell Road (from SKM, 2003).

The probability distributions of the meteorological variables at 10 m AGL in Figure 24 indicate that for wind speeds less than 4 m s^{-1} the model predictions are much less frequent than the observations, and vice versa for winds speed higher than 4 m s^{-1} (Figure 24a). These differences between the model results and the data are higher than those for the 30-m level shown in Figure 12a. In Figure 24b, there are no observed frequencies corresponding to the filtered wind sector. The model underpredicts the frequency of the northerly flow and overestimates that of the south-westerly flow. The modelled temperature probability distribution is close to the observed one, and the model performance is as good as that for the 30-m level (Figure 12c).

The model evaluation statistics in Table 11 show that the model does not predict the 10-m winds as well as those at 30 m (see Table 6). For wind speed, the index of agreement is 0.46, in contrast to 0.65 for the 30-m level winds. A further comparison analysis of the model wind predictions shows that for the 10-m level the model performs better (using index of agreement as the measure) for daytime than nighttime, and better for winter than summer. The model evaluation statistics for temperature in Table 11 are as good as those at 30 m.

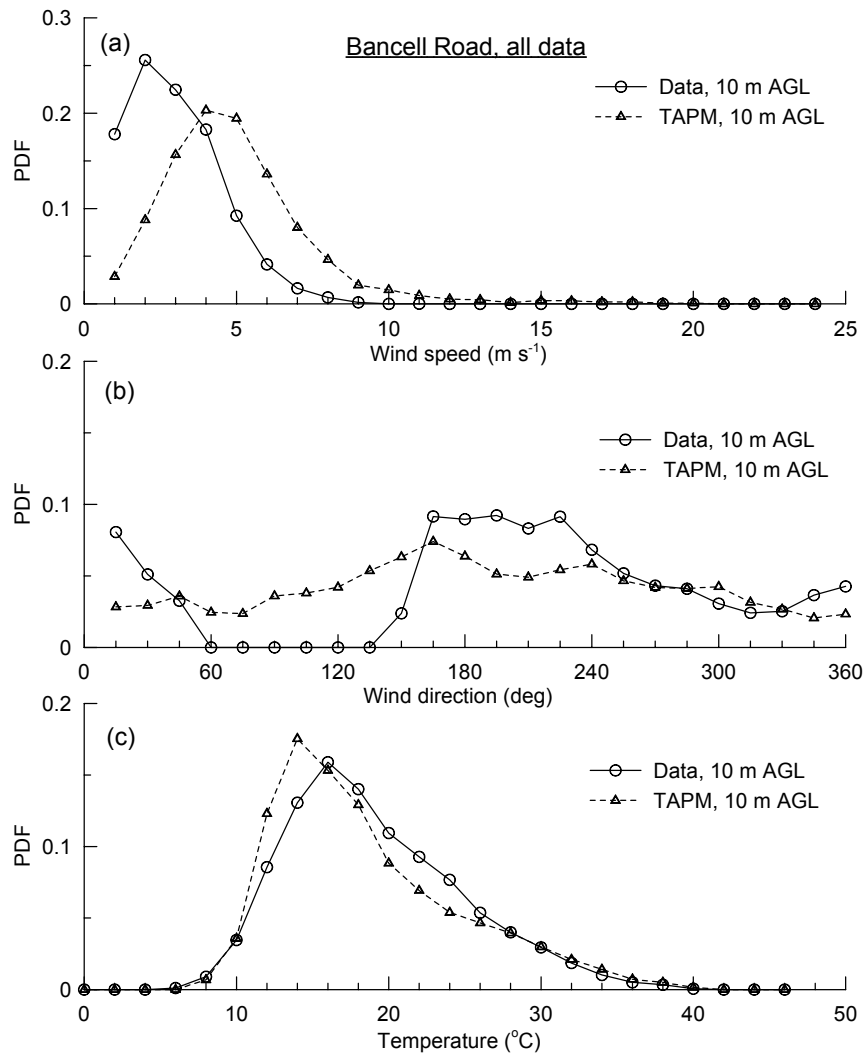


Figure 24: The observed and model probability (expressed as probability density function (pdf) of occurrence of (a) wind speed, (b) wind direction, and (c) temperature, at 10-m height at Bancell Road. The wind data corresponding to the sector 45° –145° are not included in the analysis.

Table 11: Model evaluation statistics for Bancell Road at 10 m AGL. The winds from the sector 45° –145° were not considered.

Variable	N	O_{mean}	P_{mean}	O_{std}	P_{std}	r	$RMSE$	$RMSE_S$	$RMSE_U$	IOA
WS (all)	5579	2.5	4.5	1.5	2.5	0.30	3.22	2.22	1.74	0.46
U (all)	5579	0.7	-0.4	1.6	4.0	0.56	3.50	1.24	3.27	0.55
V (all)	5579	0.2	1.0	2.4	3.1	0.88	1.72	0.86	1.49	0.90
T (all)	8342	18.1	17.6	5.8	6.1	0.94	2.13	0.44	1.86	0.97
T (day)	4208	20.1	20.4	5.9	6.5	0.96	1.88	0.30	1.81	0.98
T (night)	4134	16.0	14.8	4.8	4.1	0.91	2.35	1.36	1.67	0.93
T (winter)	4178	15.4	15.0	4.3	4.2	0.91	1.85	0.71	1.81	0.95
T (summer)	4164	20.8	20.2	5.8	6.6	0.94	2.37	0.71	2.24	0.96

6.6. Model evaluation with the Wagerup-specific land-use and Refinery heat-flux configuration – Residue Disposal Area (8 m)

The RDA site is Alcoa’s secondary weather station located about 3 km west of the Refinery (

Figure 1). Measurements of wind speed and wind direction at about 8 m AGL are made at the RDA weather station (no temperature or other data were available). Wind speed and wind direction modelled at a height of 10 m were used to compare with the observations at the RDA.

6.6.1 All data

Figure 25 presents scatter plots of model predictions vs. observed data for wind speed and wind direction at the RDA. The model is able to simulate some of the high wind speed events. The correlation coefficient for wind speed is slightly better than that at the 30-m height at Bancell Road (Figure 10).

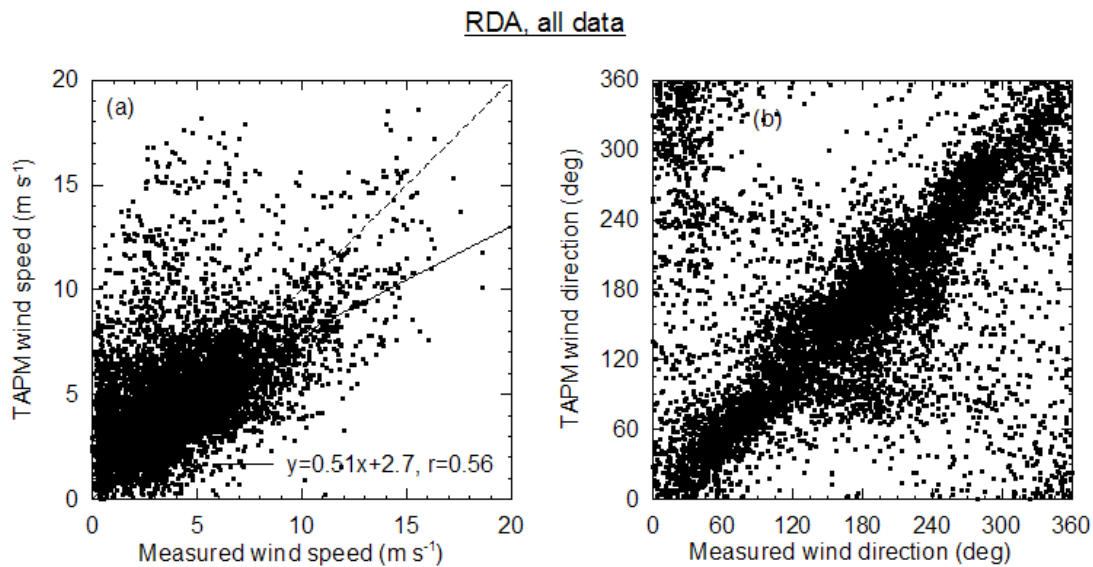


Figure 25: Scatter plots of model predictions vs. observed data for (a) wind speed, and (b) wind direction at the RDA.

Figure 26 presents the observed and model probability (or frequency) for the hourly-averaged wind speed and wind direction at the RDA for the full one year. The frequencies of wind speeds greater than 7 m s^{-1} are simulated very well by the model (Figure 26a). The model frequencies for wind speeds between $3\text{--}7 \text{ m s}^{-1}$ are higher than the observed ones. An (unusual) upturn in the observed frequency curve for the lowest wind speed range ($0\text{--}1 \text{ m s}^{-1}$) is not described by the model. The anemometer at this site is of cup type and there is a possibility that it is stalling at low wind speeds. A frequency analysis of seven years (April 1997–March 2004) of wind speed data from the RDA station by O. Pitts (personal communication, 10 September 2004) shows that the upturn in the wind speed frequency distribution for the lowest wind-speed range occurs only in the last year (April 2003–March 2004, the period simulated here), and that there is a possibility that this may be due to the degradation of the bearings in the anemometer. This may be due to the corrosive RDA environment. It is also not known whether the anemometer is serviced regularly. The stalling of the cup anemometer will underestimate the wind speed, and it can be expected that its influence would get relatively smaller as wind speed increases. However, it is difficult to estimate up to what wind speed the influence of the stalling effect extends to and what correction might be applied to the data without recalibrating the anemometer. In any case, it is clear that the model comparison would improve any such correction was to be applied.

The variation of the model frequency curve for wind direction (Figure 26b) is similar to the observed one, with the model able to predict the peaks at about 90° , 180° and 240° .

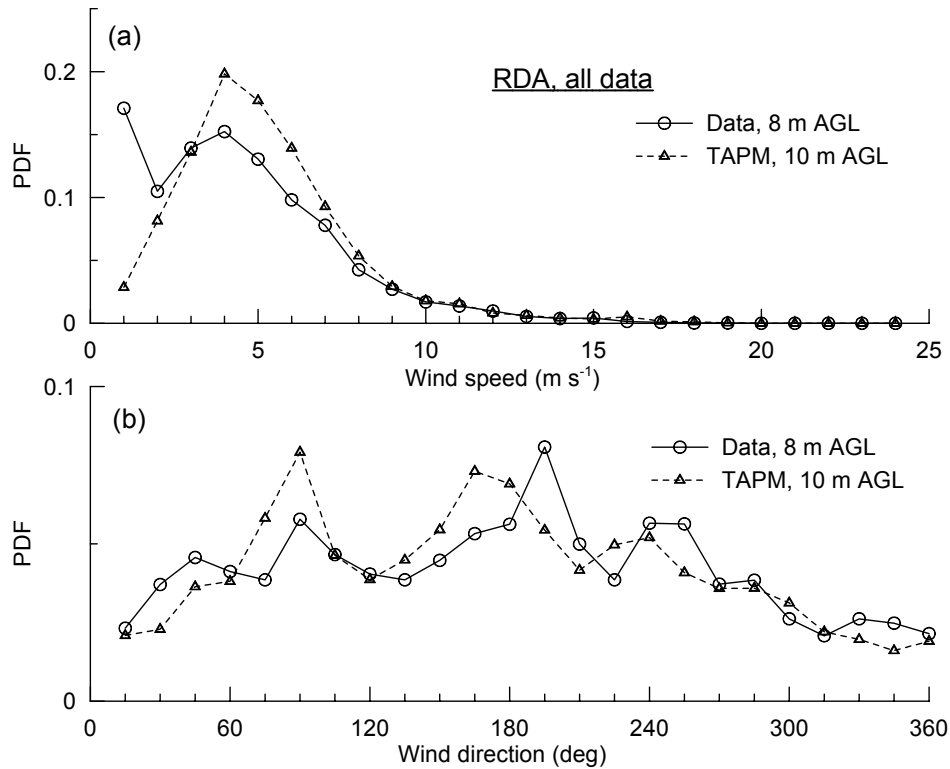


Figure 26: The observed and model probability (expressed as probability density function (pdf) of occurrence of (a) wind speed, and (b) wind direction, at the RDA.

The model evaluation statistics in Table 12 for the RDA show that the model mean wind speed is 20% stronger than the observed mean. Overall the dominant model winds (in terms of strength and frequency) are from the same quadrant (south-east) as the observed ones (which was also the case at Bancell Road). The IOA is better than that at Bancell Road, but in contrast the systematic part of the RMSE is almost of the same magnitude as the unsystematic part.

Table 12: Model evaluation statistics for RDA at 8 m AGL (TAPM winds at 10 m were used).

	Variable	N	O_{mean}	P_{mean}	O_{std}	P_{std}	r	$RMSE$	$RMSE_S$	$RMSE_U$	IOA
All data	WS	8718	4.0	4.8	2.9	2.6	0.56	2.71	1.67	1.60	0.73
	U	8718	-0.4	-1.0	3.9	4.3	0.71	3.21	1.09	3.01	0.83
	V	8718	0.4	0.8	2.8	3.1	0.82	1.84	0.54	1.76	0.90
Daytime	WS	4362	4.4	4.6	2.6	2.0	0.61	2.15	1.51	1.49	0.76
	U	4362	0.2	0.4	4.1	3.7	0.77	2.66	1.32	2.31	0.87
	V	4362	0.3	0.9	3.0	3.3	0.85	1.90	0.70	1.77	0.91
Nighttime	WS	4356	3.5	4.9	3.0	3.1	0.57	3.17	1.91	1.69	0.71
	U	4356	-0.9	-2.4	3.7	4.4	0.67	3.67	1.67	3.27	0.78
	V	4356	0.5	0.7	2.6	2.8	0.79	1.78	0.43	1.73	0.88
Winter	WS	4375	3.8	4.2	3.0	2.2	0.70	2.16	1.46	1.52	0.81
	U	4375	-0.1	-0.3	3.9	3.8	0.77	2.60	1.01	2.40	0.87
	V	4375	-0.8	-0.5	2.7	2.8	0.82	1.66	0.50	1.58	0.90
Summer	WS	4343	4.1	5.4	2.7	2.9	0.47	3.16	1.89	2.58	0.65
	U	4343	-0.7	-1.7	4.0	4.7	0.67	3.72	1.33	3.47	0.79
	V	4343	1.5	2.2	2.4	2.8	0.74	2.01	0.77	1.85	0.84

6.6.2 Daytime (0800–1900 h)

The scatter plots shown in Figure 27 for wind speed and wind direction at RDA for daytime are better than those obtained using all data (Figure 25). The model has some bias towards underestimating the high wind speeds, and overestimating the low wind speeds. The correlation coefficient for wind speed is better than that at the 30-m height at Bancell Road (Figure 13).

RDA, daytime

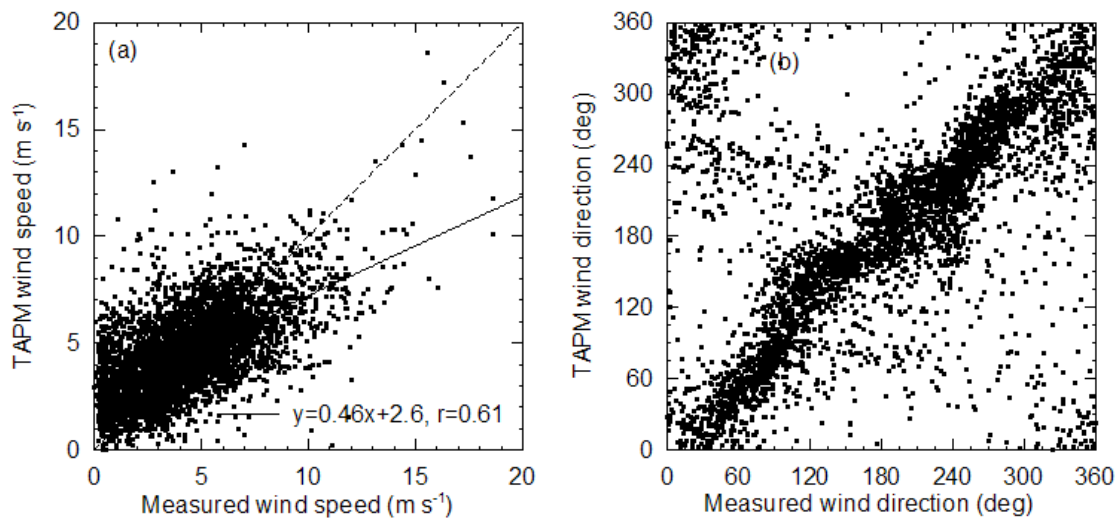


Figure 27: Scatter plots of model predictions vs. observed data for (a) wind speed, and (b) wind direction at the RDA, for the daytime.

As in Figure 26, the model frequencies for wind speeds between 3–7 m s⁻¹ in the daytime are higher than the observed ones (Figure 28a). An upturn in the observed frequency curve for the lowest wind speed value is again not described by the model. The variation of the model frequency curve for wind direction (Figure 28b) is approximately similar to the observed one, with the model able to simulate the peak at about 240°.

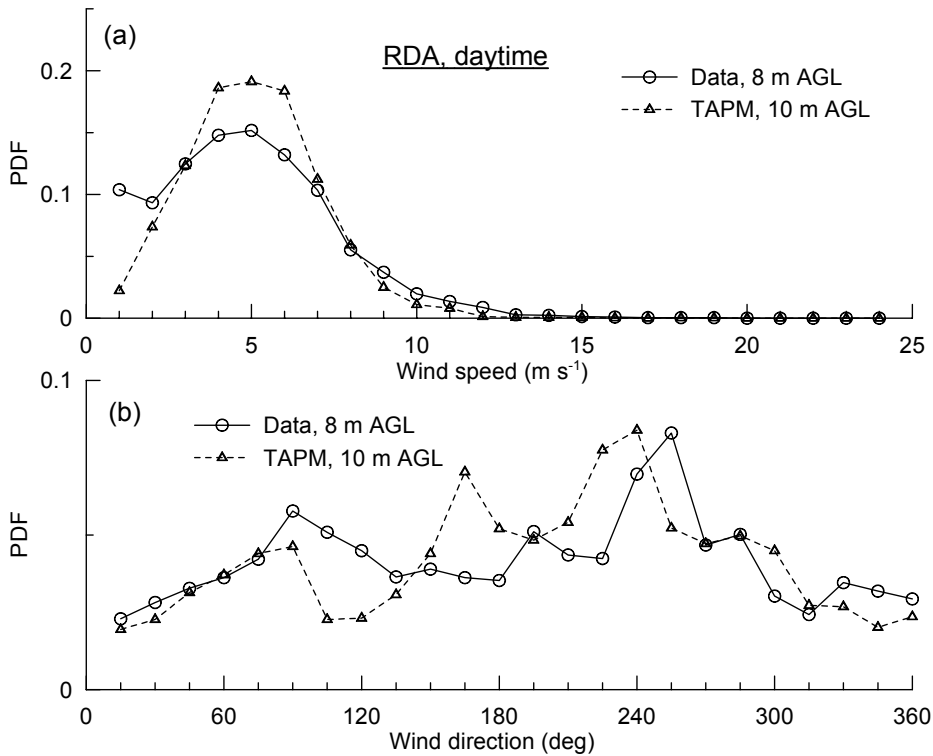


Figure 28: The observed and model probability (expressed as probability density function (pdf) of occurrence of (a) wind speed, and (b) wind direction, at the RDA for the daytime.

The model evaluation statistics for the RDA for daytime are given in Table 12. The model mean wind speed is 4.4 m s^{-1} whereas the observed mean is 4.6 m s^{-1} . The IOA is somewhat better than that at Bancell Road, but in contrast the systematic part of the RMSE is almost of the same magnitude as the unsystematic part, perhaps partly due to the unusual peak in wind speed observations for the lowest speeds.

6.6.3 Nighttime (2000–0700 h)

The scatter plots for wind speed and wind direction at RDA for nighttime are shown in Figure 29. The wind speed plot shows a slight better correlation than for Bancell Road (Figure 15).

Figure 30 presents the observed and model probability for the hourly-averaged wind speed and wind direction at the RDA for the nighttime. The unusual upturn in the observed frequency curve for the lowest wind-speed value is most prominent in the nighttime, which the model curve does not show.

The plots of the observed probability of occurrence of wind direction at the RDA and at 30 m AGL at Bancell Road are presented in Figure 30b. There are substantial differences between the two observed data curves. The frequency of south-easterly winds at Bancell Road is higher than that at the RDA. This may partly be due to downslope drainage flows from the escarpment that reach Bancell Road more often as

this site is almost in the foothills of the escarpment whereas the RDA is about 3 km west of the Bancell Road site, further away from the escarpment.

Figure 16b for Bancell Road also shows a higher frequency of modelled easterly winds than observed in the nighttime. The width of the model frequency distribution for the easterly and ESE wind directions for Bancell Road (Figure 16b) is larger than the corresponding model distribution for the RDA (Figure 30c), suggesting that the modelled easterly/ ESE flows, which may dominantly be drainage flows, are more frequent at Bancell Road than at RDA. This behaviour, which can also be seen in the corresponding observed curves (Figure 30b), is plausible, because, as mentioned earlier, the Bancell Road site is about 3 km west of the Bancell Road site, away from the escarpment.

In Figure 30c for the RDA, both data and TAPM show peaks for southerly winds, but the modelled frequency of occurrence of these winds is smaller. The model frequency curve for wind direction shows another peak corresponding to the easterly winds, which is also present in the observed curve, but the latter is almost half the size of the model value. Therefore, the nighttime easterly winds, which may include drainage flows, are predicted more frequently by the model.

The model evaluation statistics for the RDA for nighttime are given in Table 12. They are similar to those for Bancell Road (see Table 8).

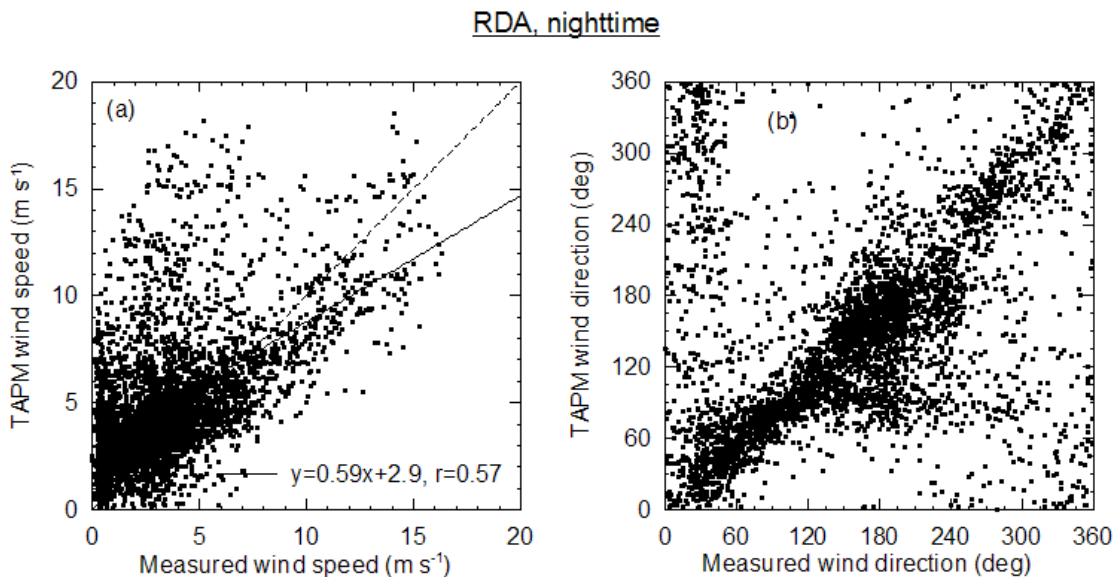


Figure 29: Scatter plots of model predictions vs. observed data for (a) wind speed, and (b) wind direction at the RDA, for the nighttime.

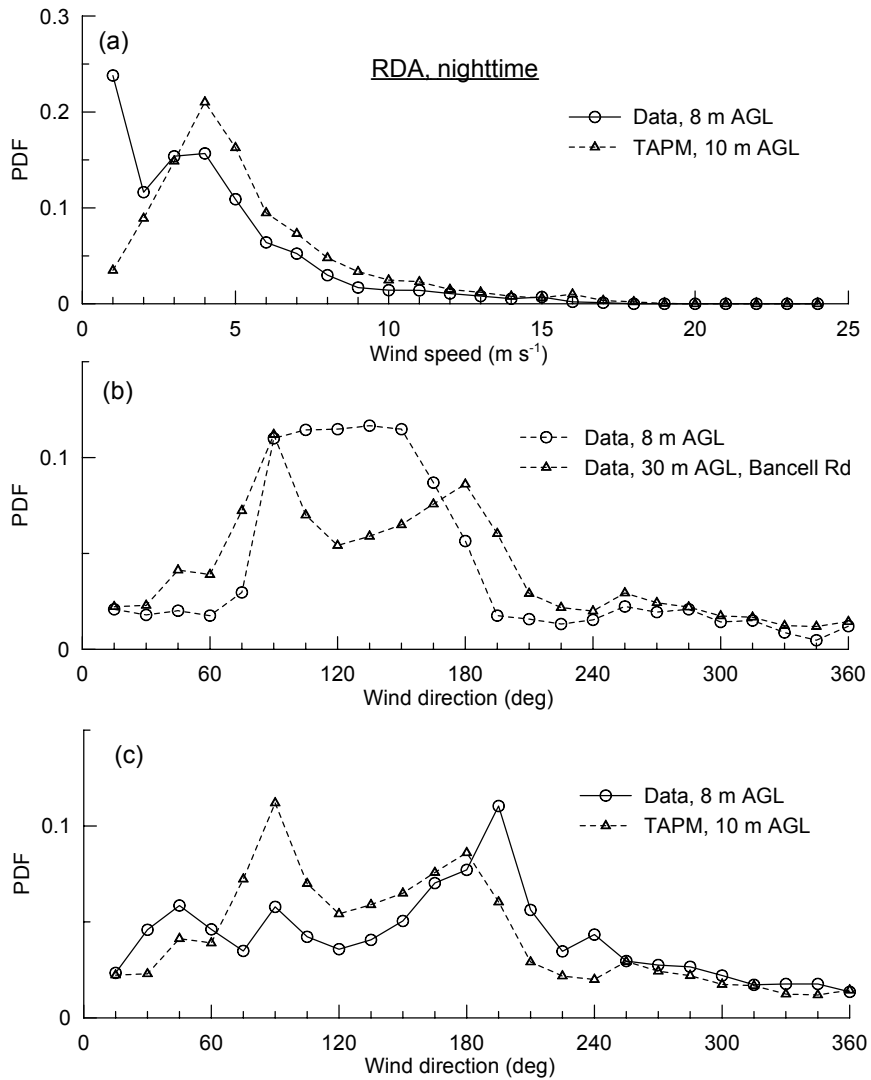


Figure 30: The observed and model probability (expressed as probability density function (pdf) of occurrence of (a) wind speed, and (c) wind direction, at the RDA for the nighttime. The observed probability of occurrence of wind direction at the RDA and at 30 m AGL at Bancell Road is presented in (b).

6.6.4 Winter period (1 April–30 September 2003)

The scatter plots for wind speed and wind direction at RDA for the winter months are shown in Figure 31.

As observed before, TAPM shows bias for underestimating the frequency of the occurrence of moderate winds (Figure 32a). TAPM simulates the observed frequency of wind direction at the RDA quite well (Figure 32b), with north-easterly winds being the most frequent.

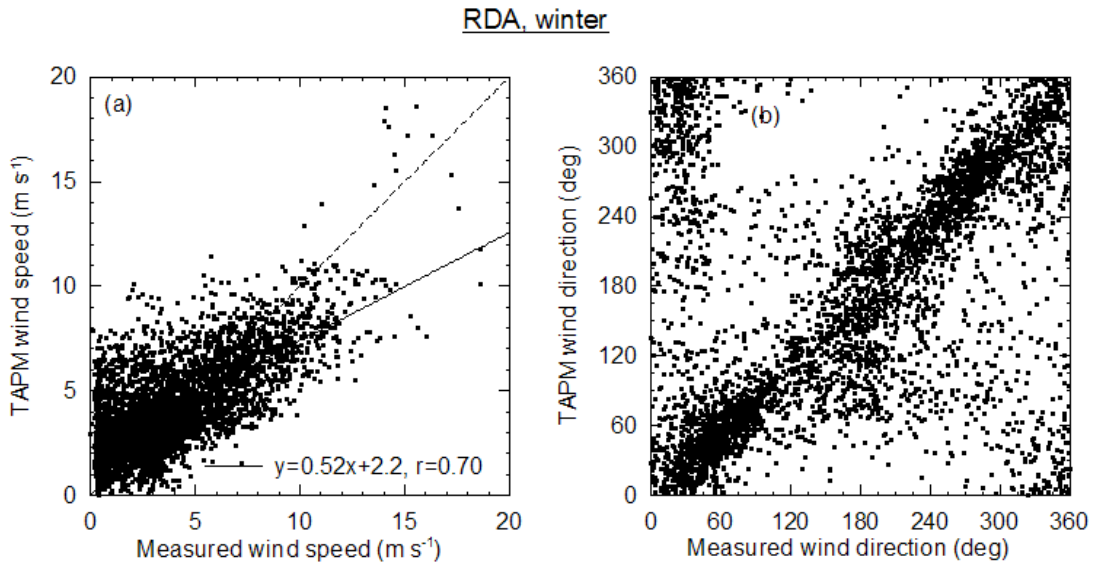


Figure 31: Scatter plots of model predictions vs. observed data for (a) wind speed, and (b) wind direction at the RDA, for winter.

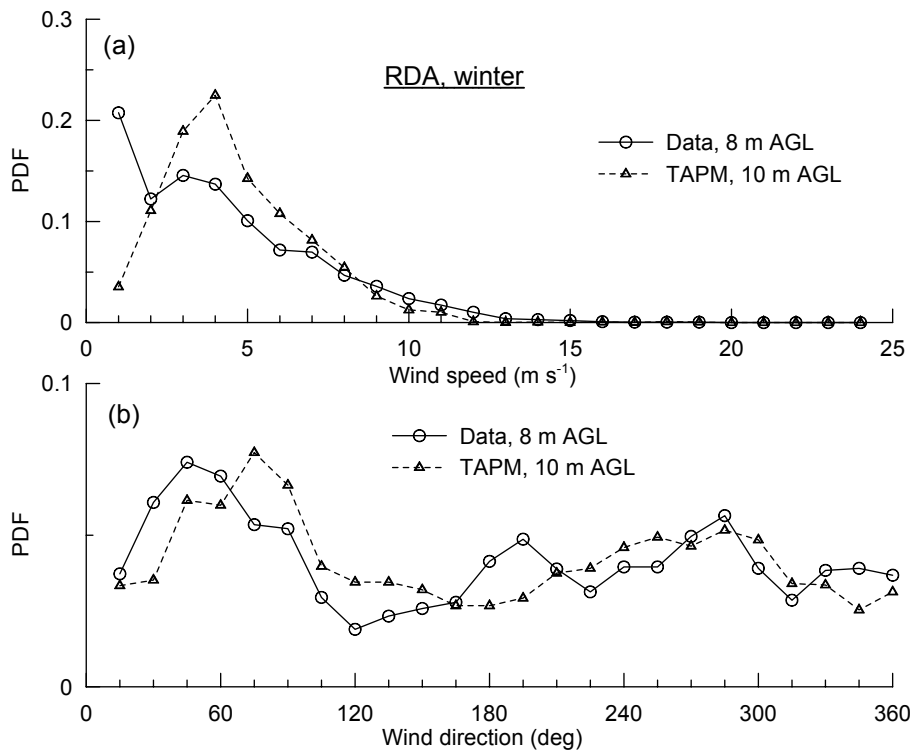


Figure 32: The observed and model probability (expressed as probability density function (pdf)) of occurrence of (a) wind speed, and (b) wind direction, at the RDA for winter.

The model evaluation statistics for the RDA for the winter period given in Table 12 are very similar to those for Bancell Road (see Table 9), but better than those for the summer time (see next Section). The signs of the U and V components suggest that the dominant model vector winds are from the same quadrant (north-east) as the observed

ones. In contrast, for Bancell Road, the signs of the modelled and observed U and V components suggest that the dominant winds are from the north-west quadrant in the winter. It is to be noted, however, the Bancell Road 30-m measurements started only from the middle of July 2003.

6.6.5 Summer period (1 October 2003–31 March 2004) including high wind speeds ($\geq 10 \text{ m s}^{-1}$)

The scatter plots for wind speed and wind direction at RDA for the summer period are shown in Figure 33. Figure 33a suggests that the wind speed is more variable than in the winter (Figure 31a)

The probability distribution curve for wind speed in Figure 34a is a little better than that for the winter period (Figure 32a). In Figure 34a, TAPM is predicting a higher frequency of wind speeds greater than 10 m s^{-1} compared to the observations. The observed wind speeds between 10–11, 11–12, 12–13, 13–14, 14–15, 15–16 and 16–17 m s^{-1} occur 1.0%, 0.9%, 0.7%, 0.5%, 0.6%, 0.2% and 0.1%, respectively, in the summer. The corresponding model probabilities are 2.1%, 1.5%, 1.2%, 0.8%, 0.7%, 1.0% and 0.3%, respectively. The TAPM simulated probability distribution of wind direction at the RDA is in good agreement with the observed distribution (Figure 34b), with southerly winds being the most frequent.

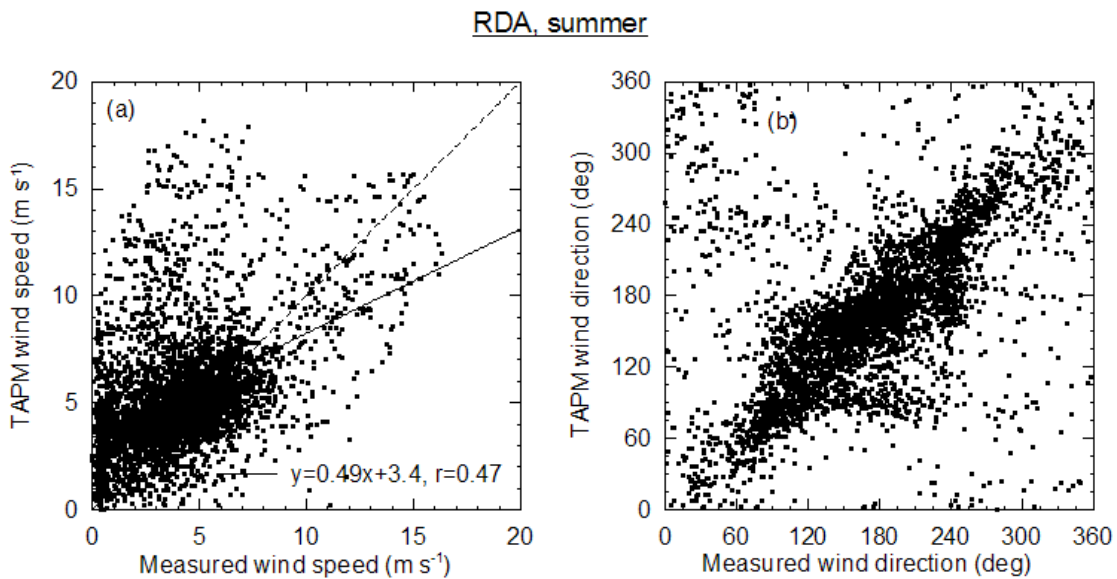


Figure 33: Scatter plots of model predictions vs. observed data for (a) wind speed, and (b) wind direction at the RDA, for summer.

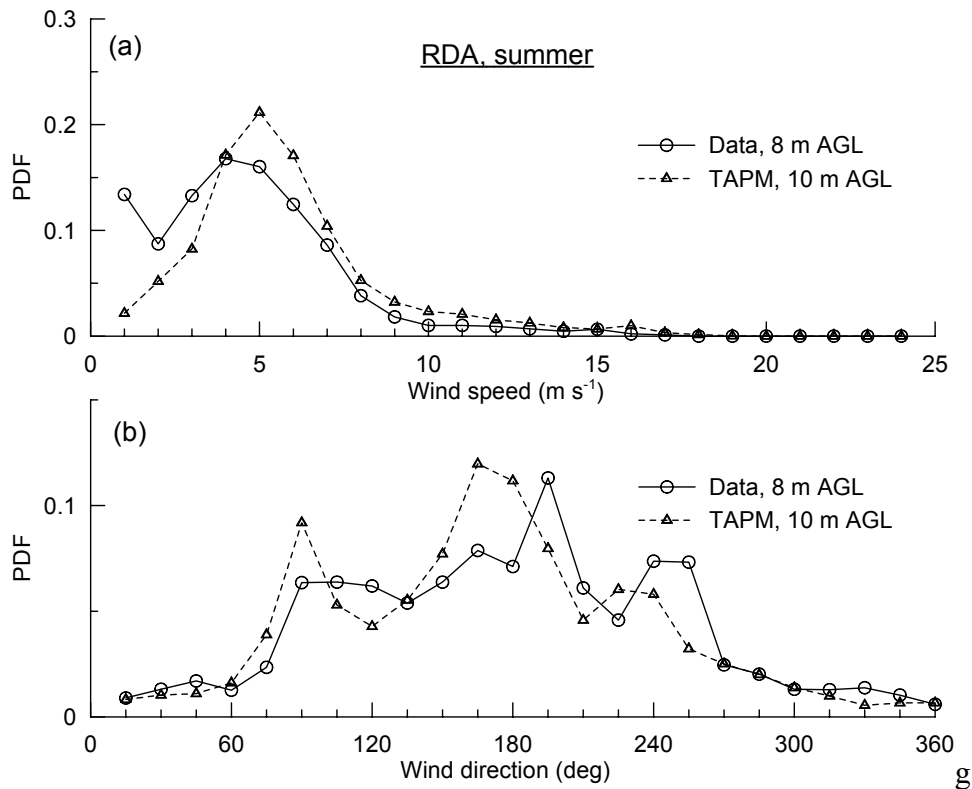


Figure 34: The observed and model probability (expressed as probability density function (pdf) of occurrence of (a) wind speed, and (b) wind direction, at the RDA for summer.

The model evaluation statistics for the RDA for the summer period given in Table 12 are similar to those for Bancell Road (see Table 10).

6.7. Prediction of the surface sensible heat flux

The surface sensible heat flux is an important quantity. The daytime surface sensible heat flux is positive (i.e. from the surface to the atmosphere) and determines the convective turbulence activity in the atmospheric boundary layer. Some of the atmospheric parameters that govern the dispersion of pollutants in the daytime are functions of surface sensible heat flux. For example, plume dispersion, as measured by the magnitude of the standard deviation of the concentration distribution, is directly proportional to the convective velocity, which in turn is proportional to the cube root of the surface sensible heat flux. The daytime boundary layer height, which limits the extent of plume dispersion in the vertical direction, is proportional to square root of the surface sensible heat flux.

Sensible heat-flux measurements are not made at Wagerup, so the TAPM predictions cannot be tested for the local area. However, a qualitative comparison of the TAPM predictions can be made with the sensible heat-flux values from measurements and applications of other models at Kwinana (about 75 km north of Wagerup). We only focus on the daytime maximum values of the sensible heat flux.

For summertime, Sawford et al. (1996) report eddy-correlation measurements of the daytime surface sensible heat flux taken during 25 January–8 February 1996 at Hope Valley in Kwinana. The peaks in these measurements generally occur during 1200–1300 h and range between 400–580 W m⁻². The maximum values of the surface sensible heat flux reported in SKM (2004) and computed using CALPUFF and the WA DEP's SOIL model for Kwinana for the period 20 February–2 March 1997 range between 400–475 W m⁻² and 240–430 W m⁻², respectively, under non-cloudy conditions. For the same period, but for 2004, at Bancell Road, the TAPM-predicted maximum values range between 400–500 W m⁻².

For the winter period 10–20 July 1997, the maximum values of the surface sensible heat flux computed using CALPUFF and the WA DEP's SOIL model for Kwinana range between 140–180 W m⁻² and 200–260 W m⁻², respectively (SKM, 2004) under non-cloudy conditions. For the same period, but for 2003, at Bancell Road, the TAPM-predicted maximum values range between 140–195 W m⁻².

Although it is not possible to make any solid conclusions about TAPM's performance for surface sensible heat-flux using values for another site and another period, the above comparison does suggest that the TAPM predictions are of comparable magnitude to other model results and data for Kwinana.

6.8. Prediction of the frequency of the near-surface northerly winds by TAPM

It is of interest to compare the frequency of the near-surface northerly winds (345°–15°) predicted by TAPM with the measurements at RDA. Under such wind directions, the Yarloop area is downwind of the Refinery, and may be impacted by the Refinery plume. It is to be noted though that the Refinery plume can reach Yarloop through other pathways when the wind is not from the north. These pathways include plume transport under nocturnal drainage flow conditions with wind direction shear, and calm winds.

The following results demonstrate that TAPM underestimates the frequency of the northerly winds, but this underestimation is much smaller at RDA than that at Bancell Road.

At 30 m AGL at Bancell Road, the measured frequencies of the northerly winds for the full year, daytime, nighttime, summer and winter are 5.5%, 4.4%, 6.6%, 2.8% and 12.2%, respectively, whereas the modelled frequencies are 2.9%, 2.7%, 3.3%, 1.3% and 7.1%, respectively. Hence, the model is underestimating the northerly wind frequency by almost a factor of two. A comparison of the frequencies of the northerly winds predicted by TAPM at 10 m AGL at Bancell Road and those obtained from the filtered wind data at 10 m at Bancell Road suggests a similar performance by the model as at 30 m.

At RDA, the measured frequencies of the northerly winds for the full year, daytime, nighttime, summer and winter are 4.4%, 5.2%, 3.7%, 1.5% and 7.4%, respectively. The corresponding TAPM-predicted frequencies are 4.0%, 4.3%, 3.6%, 1.5% and 6.4%. Hence, for these five conditions, the underestimation by TAPM of the northerly wind frequency is 9.1%, 17.3%, 2.7%, 0.0% and 1.4%, respectively.

It is hard to pinpoint the exact reasons as to why TAPM performs much better at RDA than at Bancell Road in predicting the northerly flow. A sensitivity analysis presented in

Sections 7 and 8 suggests that these differences cannot be explained by changing the surface roughness or the volumetric deep soil moisture content in the model.

The Bancell Road site is only about 1 km west from the western foothills of the escarpment, which rises to about 200 m within a distance of about 1.5 km from the foothills. The RDA site is about 4 km from the foothills. It is possible that at Bancell Road the model is not able to resolve some of the atmospheric flows forced or modified by the local topography that the wind sensor might be sampling (see Section 9 for more details). Such flows are usually highly turbulent and their complex behaviour is hard to predict. On the other hand, there are there are siting issues with the RDA site and possible stalling problems with the anemometer under low wind conditions; however, it is not immediately clear whether the wind directions measured at this site with a wind vane suffer from any stalling problems.

The synoptic weather information from the Bureau of Meteorology GASP analyses, which is a TAPM input, may also be a source of disagreement between the model results and the data for the Wagerup area.

6.9. Model comparison with radiosonde data

Section 5.2 described the radiosonde data taken in the middle of 2003. In this Section, we compare the TAPM profiles of wind speed, wind direction, temperature and relative humidity with the radiosonde data obtained on 13 July at 0801 h, on 19 July at 0727 h and 1006 h, and on 29 July at 0738 h and 1006 h WST up to a height of 1.3 km. The respective valid GPS height levels from which the observations of wind speed and wind direction started were about 45 m, 160 m, 240 m, 390 m and 120 m AGL (Pitts, 2004). The hourly-averaged model profiles chosen for comparison with the above sonde releases were at 0900, 0800, 1100, 0800 and 1100 h (end of averaging period), respectively. The sonde releases used here typically took about 4–5 minutes to reach an altitude of 1.3 km. It is worth noting that nature of sonde data is different from the way the model calculates meteorological variables. A model profile is hourly-averaged, calculated for a single surface location, and the values at all levels correspond to the same time. In contrast, a radiosonde profile involves instantaneous measurements that may not be exactly above the same surface location and are not measured exactly at the same time.

6.9.1 13 July 2003, 0801 h

Figure 35 presents the radiosonde and model profiles for 13 July 2003. The wind speed profiles show that the model is capturing the overall variation well, except for a jet at a height of about 250 m AGL, which may be a local event. The model performs very well in describing the observed the turning of the wind from the north-easterly direction to the north-westerly direction (Figure 35b). Note that the profiles of wind speed and wind direction only start from the first valid GPS level (Pitts, 2004), which was about 45 m on 13 July 2003.

The model temperature profile is reasonably close to the sonde profile (Figure 35c). (The adiabatic lapse-rate profile shown by a dotted line in Figure 35c corresponds to neutral stability conditions. A temperature profile that has a slope smaller than that of the adiabatic lapse-rate profile indicates unstable or convective conditions, whereas a greater slope suggests stable conditions.) The model temperature variation up to about 300 m is somewhat more stable than the sonde variation. The former turns to near-neutral at about 400 m, a behaviour also shown by the sonde data but from a higher

elevation of 600 m. The observed relative humidity profile is well reproduced by the model for a height of about 400 m (Figure 35d). The sharp peak at 500 m seen in the observed curve, which corresponds to the wind speed minimum just above the jet in Figure 35a, is not there in the model curve as such, but the model does show somewhat higher humidity values between 300 m and 800 m than at other levels.

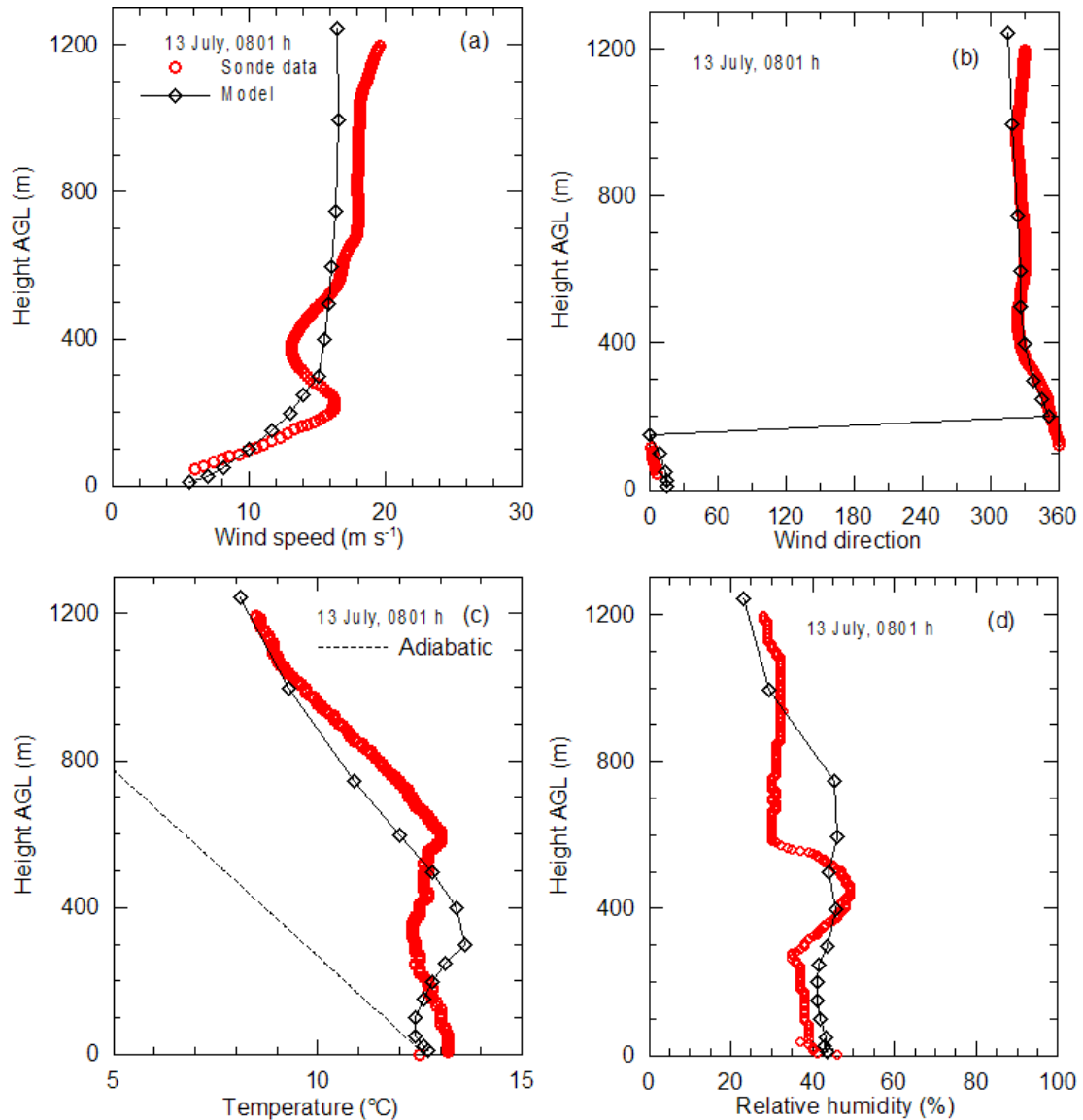


Figure 35: Profiles of meteorological variables obtained from the radiosonde releases at 0801 h on 13 July 2003, and the corresponding model profiles; (a) wind speed, (b) wind direction, (c) temperature, and (d) relative humidity. The dotted line in (c) is dry adiabatic lapse rate.

6.9.2 19 July 2003, 0727 h and 1006 h

The radiosonde profiles at 0727 h on 19 July 2003 and the corresponding model profiles are presented in Figure 36. In Figure 36a, the model is not predicting the shape of the observed wind speed profile correctly. Although, there are no wind observations below about 160 m AGL, the observed wind profile suggests the presence of a low-level jet below this height, which the model does not simulate. The observed wind direction profile in Figure 36b suggests that this low-level jet probably corresponds to flow from the escarpment. Although the model predicts flow from the escarpment in the lowest levels, the depth of this flow is shallower than what the observations suggest. The model predicts the observed anticlockwise turning of the wind with height (Figure 36b), but the model turning is not as extensive as the observed one above 500 m AGL.

In Figure 36c, the observed temperatures profile in the lowest 200 m is slightly stable with an inversion layer between 200–300 m. In contrast, the model predicts a strong inversion layer below 150 m. The model and observed variations are similar above 400 m AGL, but the model temperatures are higher. The modelled and observed relative humidity profiles in Figure 36d are qualitatively similar. However, the model predicts lower humidity than the data below 800 m.

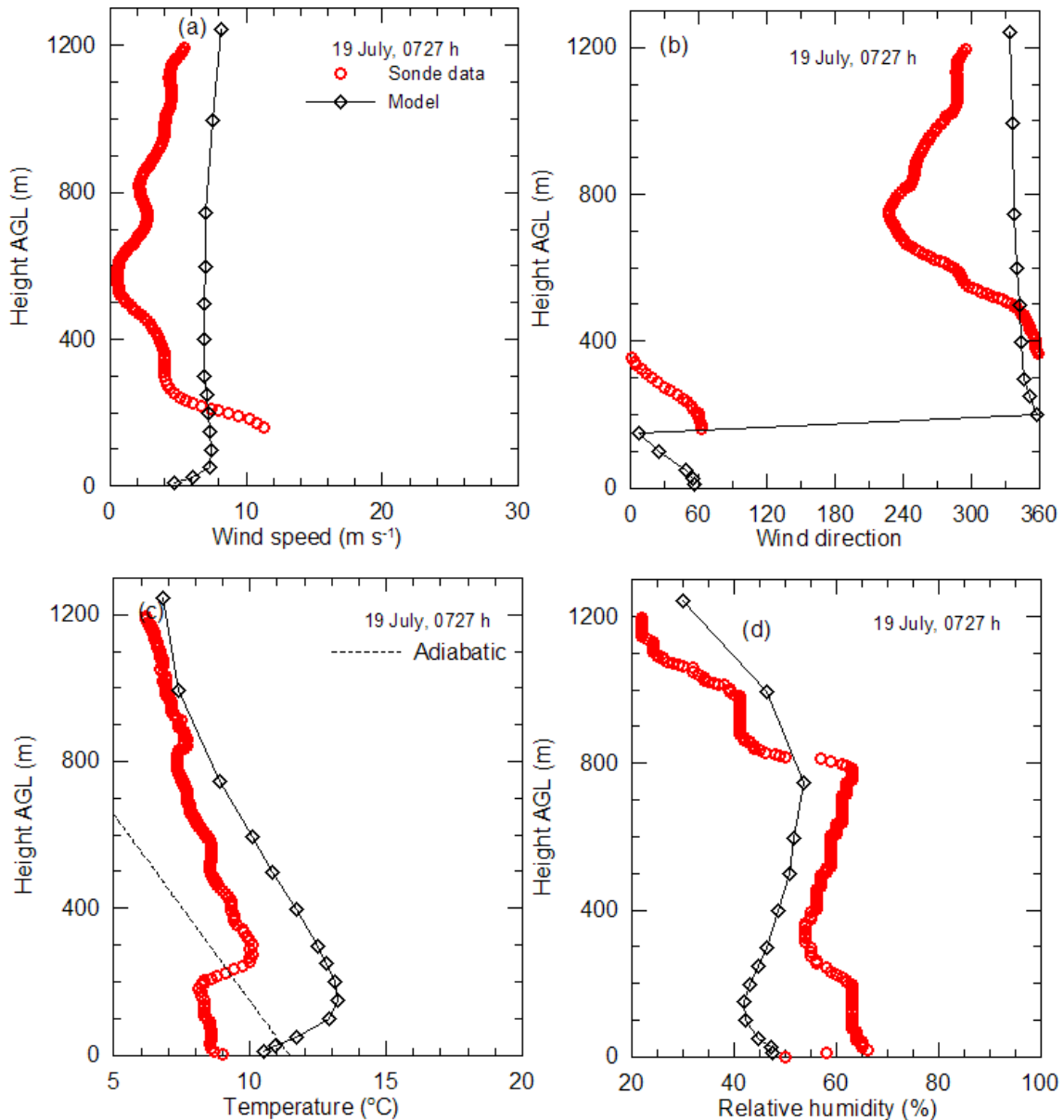


Figure 36: Profiles of meteorological variables obtained from the radiosonde releases at 0727 h on 19 July 2003, and the corresponding model profiles; (a) wind speed, (b) wind direction, (c) temperature, and (d) relative humidity. The dotted line in (c) is dry adiabatic lapse rate.

The radiosonde profiles at 1006 h on 19 July 2003 and the corresponding TAPM profiles are presented in Figure 37. In Figure 37a, the model winds speeds are higher than the sonde data. The observed turning of the wind with height in Figure 37b is clockwise, from the north-east quadrant to north-west quadrant. In contrast, the model curve indicates an anticlockwise turning from north to north-west.

The observed and modelled temperature and relative humidity profile in Figure 37c and Figure 37d are qualitatively similar. In the lowest 200 m, the model temperatures are higher by about 2.5°C. The temperature inversion at 200 m is not predicted by the model. The magnitude of relative humidity below 500 m is simulated well by the model.

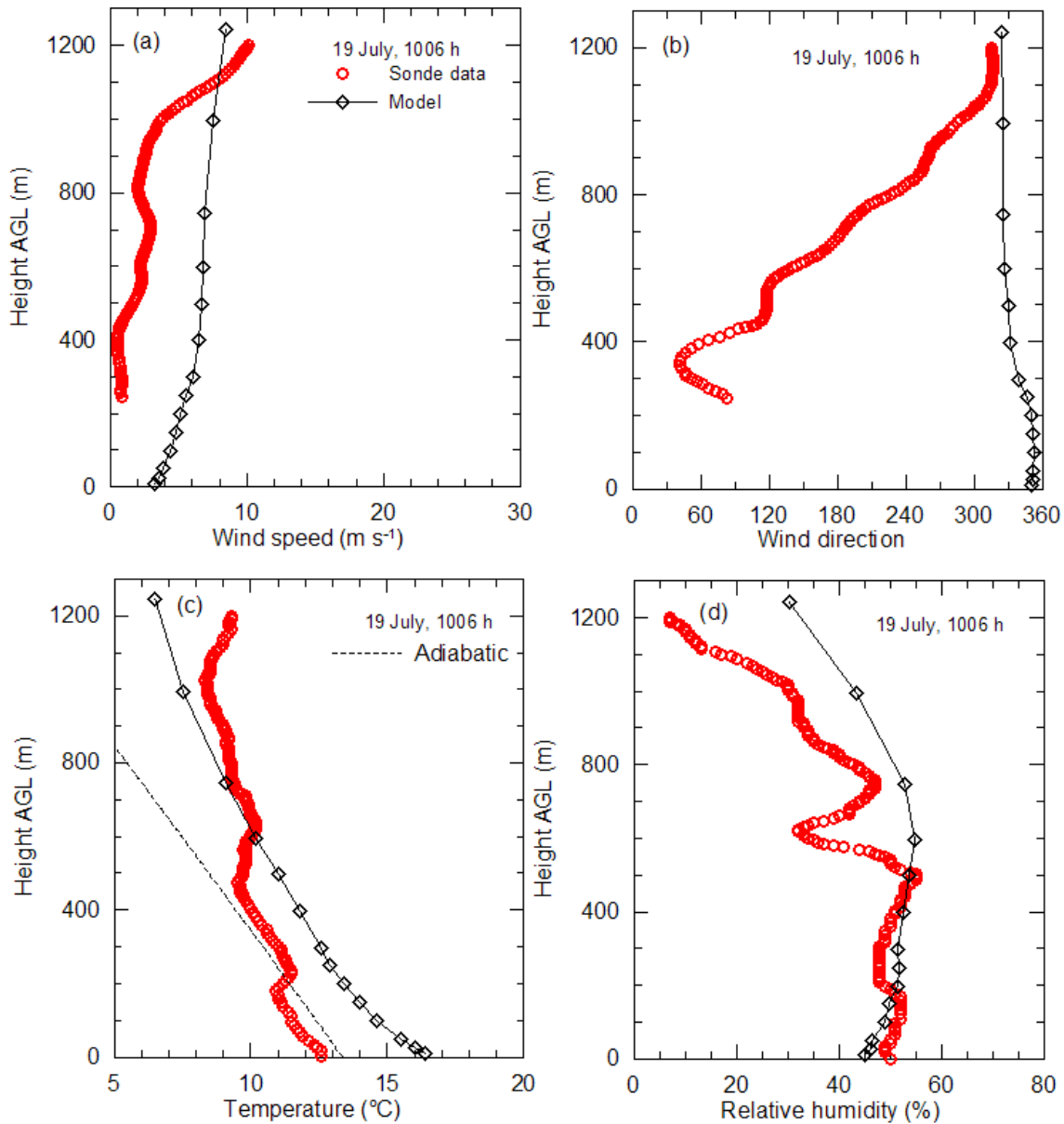


Figure 37: Profiles of meteorological variables obtained from the radiosonde releases at 1006 h on 19 July 2003, and the corresponding model profiles; (a) wind speed, (b) wind direction, (c) temperature, and (d) relative humidity. The dotted line in (c) is dry adiabatic lapse rate.

6.9.3 29 July 2003, 0738 h and 1006 h

The radiosonde profiles at 0738 h on 29 July 2003 and the corresponding model profiles are presented in Figure 38. The lowest GPS level for the observed winds in Figure 38a and Figure 38b is about 390 m. It is clear that the model predicts stronger winds than the observations and shows a low level jet at 300 m with a speed of 23 m s^{-1} . A jet at 450 m with a speed of 18 m s^{-1} can also be observed in the sonde profile. The model is able to simulate the observed turning of the wind with height from north-easterly to northerly (Figure 38b).

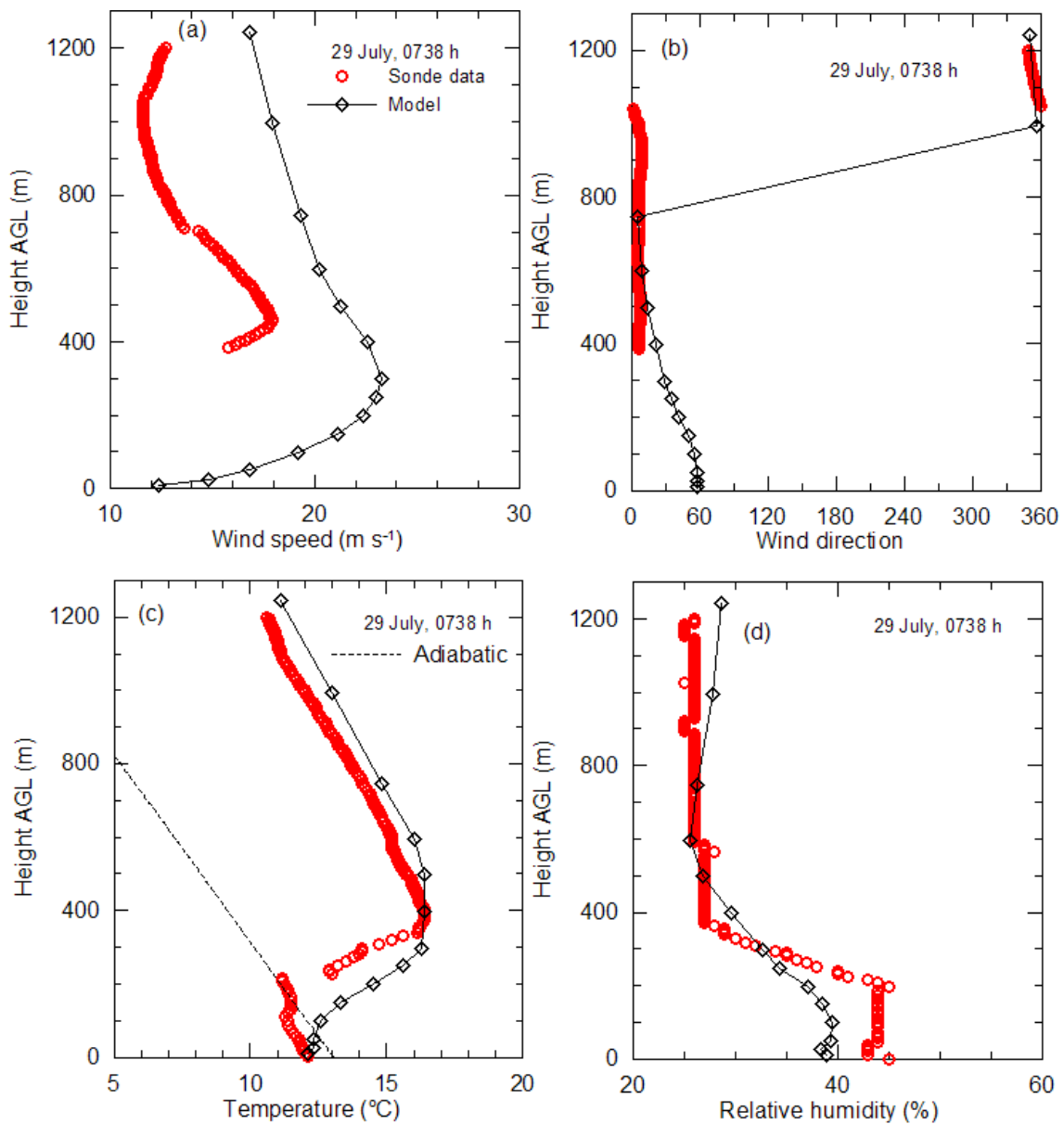


Figure 38: Profiles of meteorological variables obtained from the radiosonde releases at 0738 h on 29 July 2003, and the corresponding model profiles; (a) wind speed, (b) wind direction, (c) temperature, and (d) relative humidity. The dotted line in (c) is dry adiabatic lapse rate.

The temperatures profiles in Figure 38c indicate that in the lowest 200 m the sonde profile is weakly stable (or near neutral) whereas the model curve is strongly stratified. The data show a sharp inversion at about 200 m, which the model also predicts, but at a lower height and with a somewhat weaker strength. The model performs very well for heights above 350 m. The model is doing a good job at describing the sonde relative humidity profile in Figure 38d.

Figure 39 shows the sonde and model profiles at 1006 h on 29 July. The lowest GPS level for the observed winds in Figure 39a and Figure 39b is about 120 m. Overall, the model wind speed profile is qualitatively similar to the sonde one, with the wind strengthening with height and then weakening at higher altitudes. The model winds are stronger below 700 m and weaker above. Figure 39b demonstrates a very good performance by the model in simulating wind direction and its turning with height. The temperature profiles in Figure 39c demonstrate a respectable performance by TAPM in describing the weakly-stable layer below 150 m and the inversion above it. However, between 400 m and 800 m, the model performance is not as good. The model relative humidity in Figure 39d is, on average, lower by a magnitude of 15% than the data, but the overall shape of the model profile is not too different from the sonde data.

Some the differences between the model and observed sonde profiles arise because, as mentioned before, the former are hourly-averaged values at a single surface location (corresponding to the sonde release site) with the values at all levels correspond to the same time, whereas the latter are instantaneous measurements that may not be exactly above the same surface location and are not measured exactly at the same time. These spatial and temporal differences are expected to be larger over complex terrain (e.g. Wagerup) than over flat terrain because of the spatial inhomogeneities in terrain changing regional flow patterns and even generating local flows with relatively small time scales.

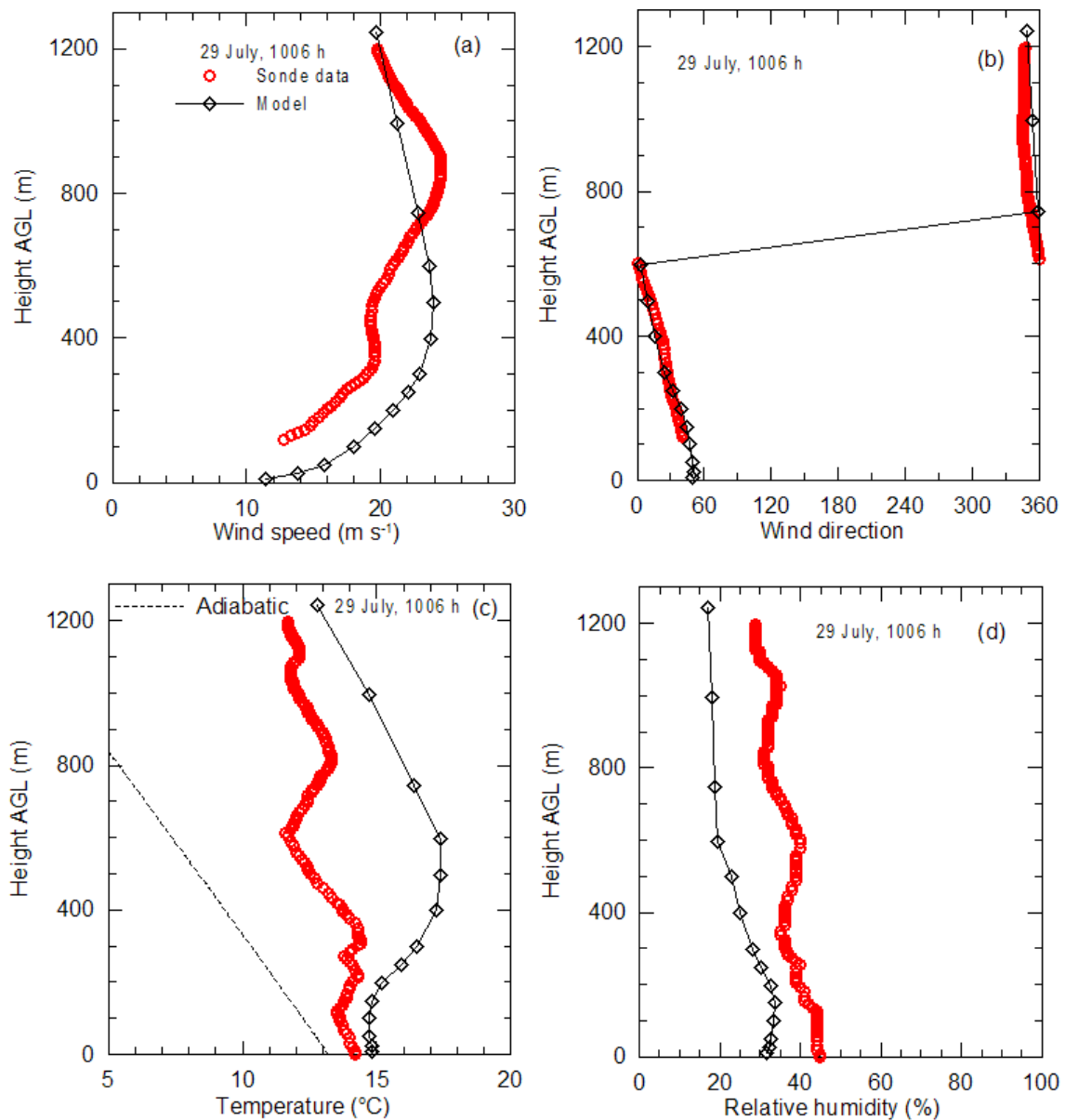


Figure 39: Profiles of meteorological variables obtained from the radiosonde releases at 1006 h on 29 July 2003, and the corresponding model profiles; (a) wind speed, (b) wind direction, (c) temperature, and (d) relative humidity. The dotted line in (c) is dry adiabatic lapse rate.

7. Sensitivity of TAPM meteorology to surface roughness

This sensitivity of TAPM to surface roughness length should show whether the differences between the modelled meteorology and the measurements obtained above in this report can, to an extent, be explained by some degree of variation in the value of surface roughness length.

In the runs presented previously, TAPM used Equation (1) for calculating the surface roughness length (z_o) for vegetation cover. In this section, the sensitivity of TAPM is tested for enhanced surface roughness by using the following scheme:

$$z_o = \min[0.1 + (h_f / 10), 2.0], \quad (2)$$

In Equation (2), the minimum value of z_o is 0.1 m, whereas the maximum value is 2.0 m. Due to the reasons given in Section 3.2, the lower and upper limits cannot be varied greatly. Figure 40 presents the variations of z_o with the height of the roughness element (h_f) calculated using Equation (1) and Equation (2).

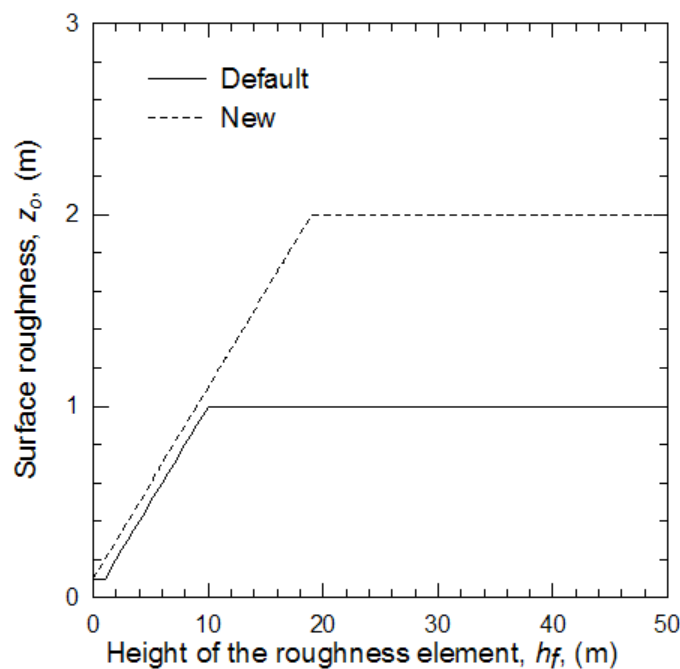


Figure 40: The variation of the surface roughness length (z_o) with the height of the roughness element (h_f) in TAPM; solid line – default scheme (Equation (1)), and dashed line – new scheme (Equation (2)).

The main difference between Equation (1) and Equation (2) in the context of Wagerup is that the two land-use categories Forestry (covering 42% of the area), and Water production, mining, recreation (covering 14.2% of the area) (see Table 2) both now have a roughness length of 1.8 m instead of the 1.0 m.

The modelled probability distributions of wind speed, wind direction, temperature, net radiation, and relative humidity at Bancell Road obtained using the surface roughness length schemes (1) and (2) for the period 1–31 August 2003 are shown in Figure 41. The differences between the model meteorological curves obtained using the two roughness schemes are not significant. They would not explain the differences between the modelled meteorology and the observations in Figure 12.

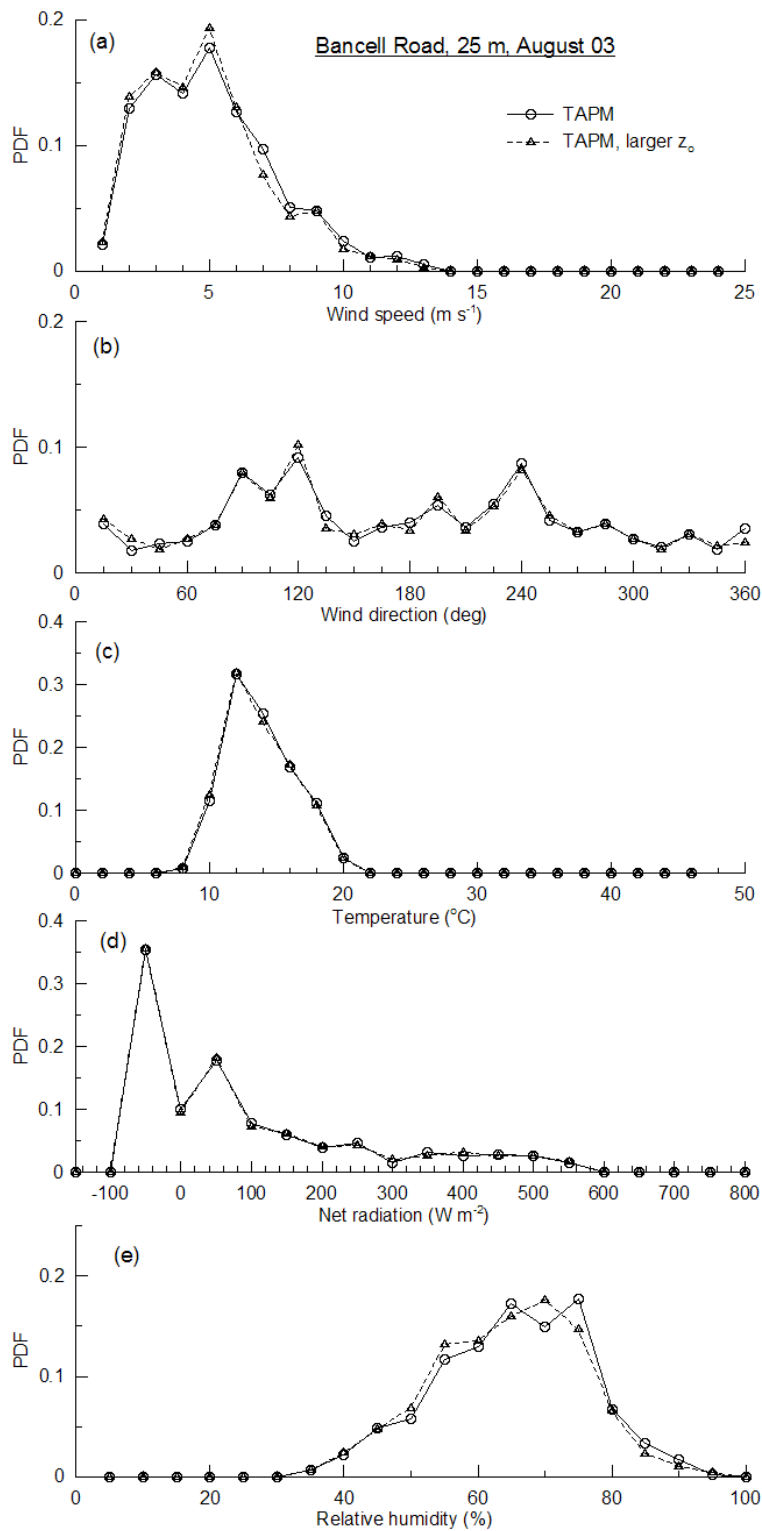


Figure 41: The model probability (expressed as probability density function (pdf)) of occurrence of parameter values for (a) wind speed, (b) wind direction, (c) temperature, (d) net radiation, and (e) relative humidity at Bancell Road obtained using the default surface roughness length and a larger surface roughness length for the month of August 2003. The net radiation and relative humidity are determined at 1.5 m AGL while the other parameters are determined at 25 m AGL.

8. Sensitivity of TAPM meteorology to deep soil volumetric moisture content

The deep soil volumetric moisture content (at a depth of about 1 m from the surface) affects thermal properties of soil, thereby influencing the meteorology of an area through the lower boundary condition in the model. In the TAPM results presented earlier in this report, the deep soil volumetric moisture content (η_d) in units of $\text{m}^3 \text{m}^{-3}$ (i.e. volume of water per volume of soil) was set to the default value of 0.15, which is a reasonable value to use for most times of the year in regions dominated by sandy clay loam soil. In the model, the value of deep soil moisture content can be specified for each month. Generally, for sandy soils and dry months a lower value (e.g., 0.05–0.10), and for clay soils and wet months a higher value (e.g., 0.20–0.25) may be appropriate. However, generally, no direct measurements of η_d are taken. Some of the previous applications of TAPM for other areas in which non-default values of η_d were used involved trial and error so that the selected values of η_d led to model results that matched observations to a greater degree than when the default value was used.

The values of η_d used in other TAPM studies for Western Australia include: a constant value of 0.15 at Kwinana for an annual run for the year 1997 (Hurley et al., 2001), 0.05 in the summer months to 0.25 in the winter months at Kwinana for the same period (Hurley et al., 2002), a constant value of 0.1 for the Pilbara region for the year 1999 (Hurley et al., 2003b), and Collie ranging from 0.1 to 0.2 (Hibberd et al., 2003).

In this section, the sensitivity of TAPM to the deep soil moisture content for Wagerup is tested by running TAPM with $\eta_d = 0.25$ for the winter month of August 2003 and $\eta_d = 0.05$ for the summer month of January 2004. This sensitivity should reveal whether the differences between the modelled meteorology and the measurements obtained above can be explained by the deep soil moisture content in the model.

The modelled probability distributions of wind speed, wind direction, temperature, net radiation, and relative humidity obtained at Bancell Road for the two values of deep soil moisture content ($\eta_d = 0.15$ (default) and 0.25) for the period 1–31 August 2003 are shown in Figure 42. The net radiation and relative humidity are determined at 1.5 m AGL while the other parameters are determined at 25 m AGL. The model curves indicate that the differences between the model curves are not significant, except for relative humidity. There is an increase in the frequency of high relative humidity values (> 60%) and a decrease in the frequency of low relative humidity values when $\eta_d = 0.25$. The model results in Figure 42 suggest that making deep soil moisture content higher in winter would not explain the differences between the modelled meteorology and the observations in Figure 19

Figure 43 shows the same model variables as in Figure 42 but for the summer month of January 2004 with $\eta_d = 0.15$ (default) and a drier value of $\eta_d = 0.05$. Again, except for the relative humidity, the differences between the two model curves are small. The relative humidity predictions for summertime in Figure 21 are already good. Therefore, it can be concluded that a decrease in the value for the deep soil moisture content would not explain the differences between the modelled meteorology and the observations in Figure 21 for summertime.

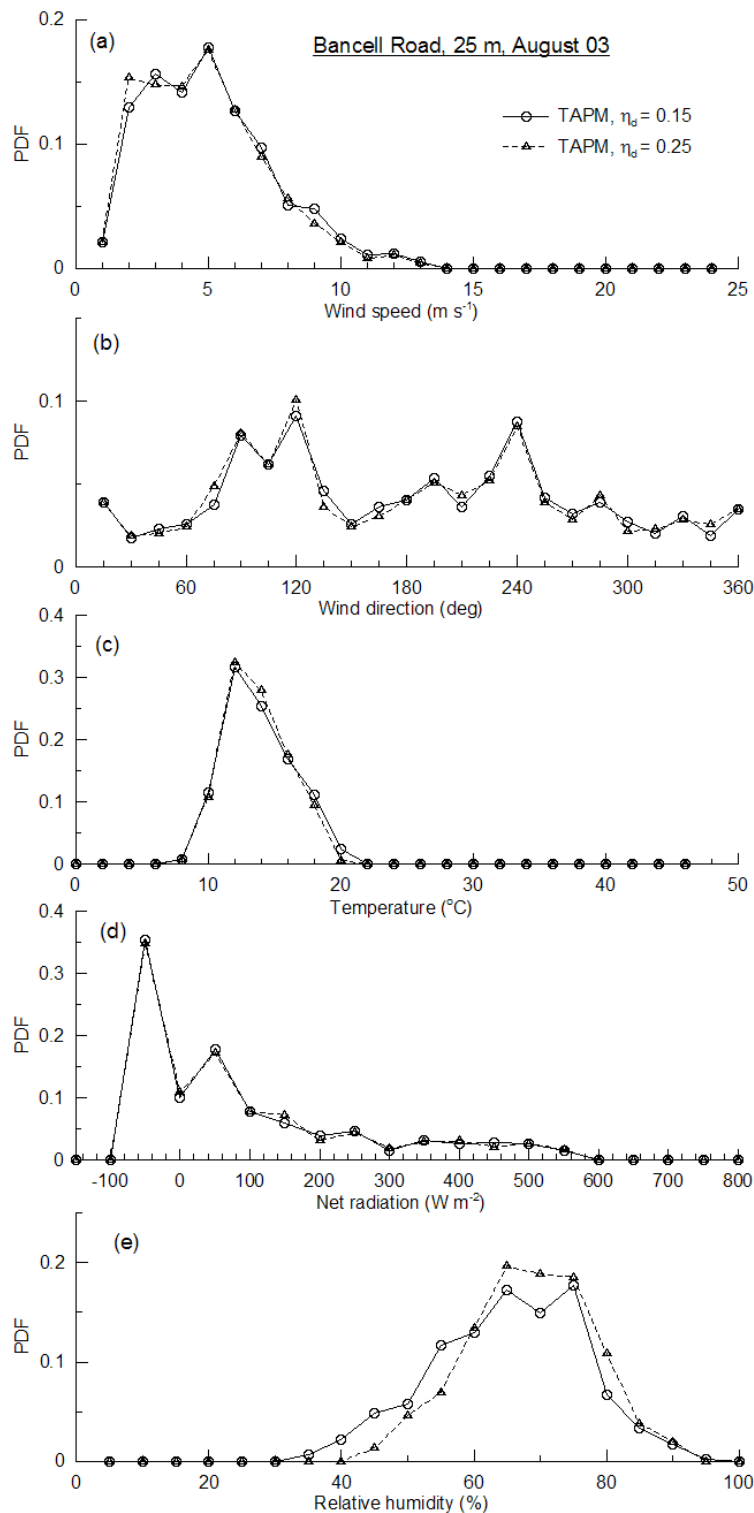


Figure 42: The model probability (expressed as probability density function (pdf)) of occurrence of parameter values for (a) wind speed, (b) wind direction, (c) temperature, (d) net radiation, and (e) relative humidity at Bancell Road obtained for two values of the deep soil moisture content, $\eta_d = 0.15$ (default) and 0.25 for the month of August 2003. The net radiation and relative humidity are determined at 1.5 m AGL while the other parameters are determined at 25 m AGL.

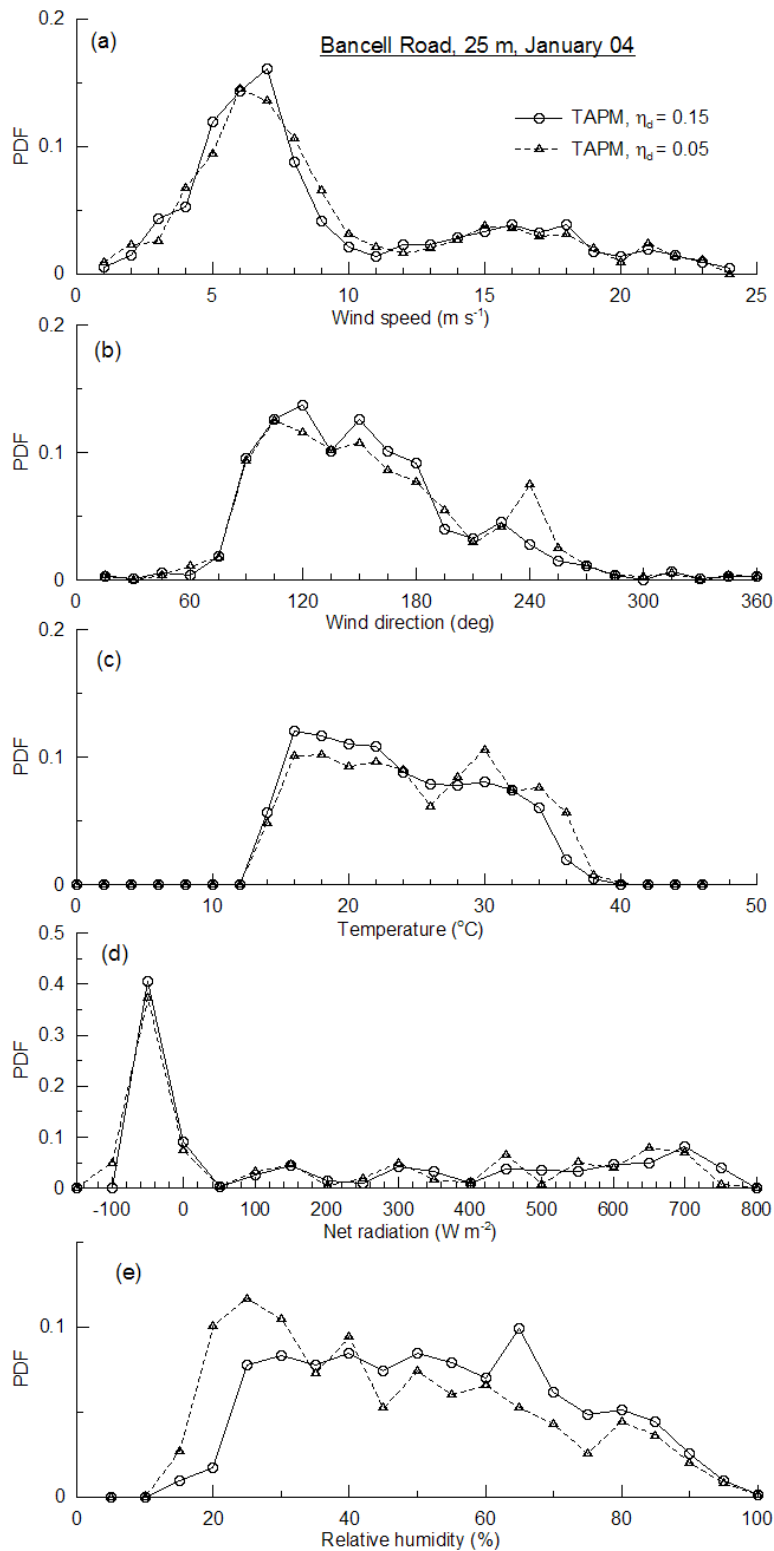


Figure 43: The model probability (expressed as probability density function (pdf)) of occurrence of parameter values for (a) wind speed, (b) wind direction, (c) temperature, (d) net radiation, and (e) relative humidity at Bancell Road obtained for two values of the deep soil moisture content, $\eta_d = 0.15$ (default) and 0.05 for the month of January 2004. The net radiation and relative humidity are determined at 1.5 m AGL while the other parameters are determined at 25 m AGL.

9. Some sources of disagreement between the model results and the data

The predictions from all models of physical processes have uncertainty associated with them. Some models such as those that predict the movement of the earth around the sun have very small uncertainties. Other models such as those used for the numerical weather prediction have large uncertainties. The following describes some possible sources of uncertainty in the TAPM modelling at Wagerup.

The mathematical equations which describe the motions of the atmosphere are based on the fundamental laws of motion (proposed by Sir Isaac Newton) and the laws of thermodynamics. A realistic representation, or “model”, of the atmosphere gives rise to equations which are too complicated to be solved by ordinary mathematical methods. As a practical approach to this problem approximations to these equations are created, which can be solved numerically on a computer. The computer programs which find these approximate solutions are called “numerical models”, and TAPM is such a model. Even when the fastest computers are used, numerical models are only approximations of the full dynamic and thermodynamic equations. Their solutions are therefore also only approximations. There is no atmospheric model as yet that can be used for practical applications while at the same time solve the mathematical equations in their most accurate form.

The performance of an atmospheric model also depends strongly on the accuracy of the boundary conditions. The synoptic weather information from the Bureau of Meteorology GASP analyses, which is used as a boundary condition in TAPM, may also be a source of uncertainty and, consequently, of disagreement between the model results and the data for the Wagerup area. The GASP information is obtained from the output a meteorological model with assimilation of meteorological observations from a network of stations.

Predictions are also dependent upon the temporal and spatial resolution of the model and of the input data. Generally, the higher the resolution the better the predictions. The TAPM resolution for meteorology used in this report is 0.5 km, which is twice the resolution used in most previous applications of TAPM. Any further increase in the resolution is unfeasible from the point of view of computer processing time as the doubling the resolution would normally require four times the computer processing time.

We find one particular reason that could cause part of the model-observation disagreement could be the complex air flows associated with the topography near the Refinery. The Bancell Road meteorological station is close to the escarpment and this site is influenced by effects of the escarpment. The RDA is further from the escarpment and so is probably not influenced by the escarpment as much.

Past meteorological and fluid dynamics studies (Oke, 1987) have shown that for a steep topography when the upwind or downwind slope of the ground exceeds about 0.3 (17°), flow separation occurs (i.e. the flow does not adjust to the underlying topography), accompanied by local secondary flows such as eddies. For example under neutral atmospheric conditions, flow up an escarpment can produce: a bolster eddy at the base; strong jetting over the escarpment edge due the flow constriction in the vertical; and often a lee eddy on the top slightly back from the edge, which is a site conducive to convective cloud formation (as a result of the warm moist air lifting up the escarpment

face and then cooling down) (see Figure 44). Flow down the escarpment will cause a deceleration, and create a strong lee eddy. At the base of the escarpment, winds can be counter to the mean flow, unsteady and turbulent. Hence this area is sheltered with weak mean winds but subject to intermittent gustiness. The above effects will be dampened under stable conditions, and enhanced under unstable conditions. When the flow is not normal to the escarpment, the strength and persistence of these flow features will be reduced. Such complex systems are difficult to describe mathematically in models for practical applications such as air pollution studies.

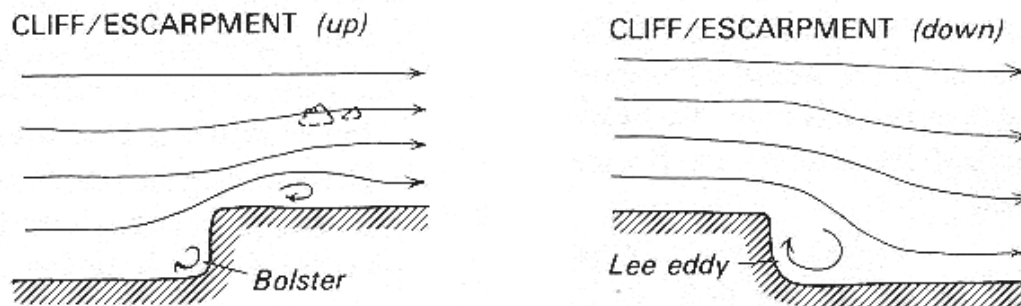


Figure 44: Typical patterns of airflow over an escarpment (from Oke, 1987).

The Darling escarpment east of Wagerup is not as steep as a slope of 0.3 (at the most 0.2), but it is possible that the Bancell Road site, which is about 1 km from the foothills of the escarpment, is influenced by some of the above features. Such an influence is evident in Figure 45 which shows the variation of the observed hourly-averaged standard deviation (σ_θ) of wind direction with the observed hourly-averaged wind direction at 30-m AGL at Bancell Road. The σ_θ data were binned in the wind direction bins of 5–15, 15–25, 25–35...etc, and the σ_θ values in each bin were averaged. In Figure 45, the σ_θ averages are plotted against the mid-values of the wind-direction bins. The quantity σ_θ is a measure of the gustiness or unsteadiness of the flow, the higher its value the greater the gustiness. Generally, the lower the hourly-averaged wind speed the higher the hourly-averaged σ_θ value. Figure 45 indicates that σ_θ peaks when the flow is upwind or downwind of the escarpment, suggesting the turbulent nature of the flow under these conditions.

TAPM cannot resolve some of the above features such as leeward and windward eddies and the associated gustiness. The sheltering at the base of the escarpment not predicted by the model will lead to an overestimation of the wind speed by the model. Formation any clouds along the ridgeline that is not predicted by the model will lead to an overestimation of the net radiation by the model during the morning hours. However, as mentioned before, these local effects are difficult to formulate for inclusion in a meteorological model.

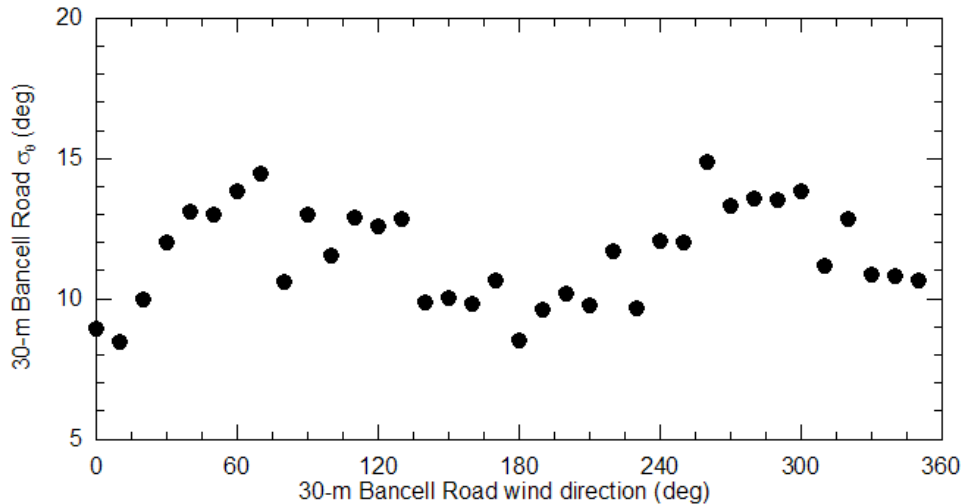


Figure 45: Variation of the observed standard deviation (σ_θ) of the wind direction with the observed wind direction at 30-m AGL at Bancell Road.

Another reason for the model not being able to predict the low wind speeds (this may also cause errors in the wind direction predictions) is the limitations of the existing similarity laws as used in TAPM (and most other prognostic meteorological models). Boundary conditions are specified at the first model level (i.e. 10 m AGL) using scaling laws based on similarity theories that are the basis of the science of micrometeorology (the meteorology of the small-scale motions within the atmospheric boundary layer (ABL)). To keep consistency with these laws, certain restrictions need to be imposed on meteorological variables. Such restrictions include the mean wind speed to be always greater than or equal to 0.5 m s^{-1} ; and the micrometeorological parameters the Obukhov length (L) to be always greater than the first model level, and the friction velocity (u_*) to be between $0.05\text{--}1.0 \text{ m s}^{-1}$. This means that close to the surface, the model cannot predict wind speeds less than 0.5 m s^{-1} , and very stable nighttime conditions for which $L < 10 \text{ m}$. The model assumes that the flow is always turbulent, and the low frequency meandering of the wind under low/calm winds is not accounted for. The following example illustrates this.

Figure 46a shows a scatter plot of the TAPM 10-m wind speed vs. TAPM 25-m wind speed at Bancell Road. As expected, the 10-m wind speeds are generally lower than the 25-m wind speeds. The ratio of the 25-m wind speed to the 10-m wind speed, as determined from a regression line (solid line) passing through the origin, is calculated to be 1.19, and is almost independent of the range of wind speeds (e.g. low or high wind speeds) selected. This ratio is very close to the value 1.20 obtained from the well-known logarithmic wind profile based the surface similarity theory for neutral conditions, assuming a roughness length (z_o) of 0.1 m (the same value as used by TAPM for the Bancell Road area).

Figure 46b shows a scatter plot of the observed 10-m wind speed vs. observed 30-m wind speed at Bancell Road. (Note that the 30-m measurements started from 18 July 2003.) In this figure, the wind data corresponding to the sector $45^\circ\text{--}145^\circ$ were not

included because of the sheltering of the 10-m wind sensor. It is clear that the observed overall drop in wind speed from the 30-m level to the 10-m level is much greater than what the model shows in Figure 46a. The ratio of the observed 30-m wind speed to the observed 10-m wind speed for the wind speed range $0.5\text{--}2\text{ m s}^{-1}$ (as determined from a regression line (solid line) passing through the origin) is 2. The observed ratio decreases with wind speed. For example, it is 1.57 for the wind speed range $2\text{--}5\text{ m s}^{-1}$, and 1.38 for wind speeds above 5 m s^{-1} . These ratio values are larger than the value 1.24 obtained from the logarithmic wind for neutral conditions for $z_o = 0.1\text{ m}$ (there are stability corrections to the logarithmic wind profile but these variations are distributed around the behaviour for neutral conditions). Even if the value of z_o is increased to 0.3 m , the ratio obtained from the logarithmic wind profile increases to only 1.31.

The above analysis shows that as the wind speed decreases there is more and more departure of the observed wind speed from the behaviour predicted by the surface similarity theory. Unfortunately, no theory has been developed to cover these low wind conditions (normally associated with very stable conditions) where turbulence either ceases or becomes intermittent and similarity theory no longer applies. No practical method of modelling these conditions currently exists.

In summary, two reasons why the model is not predicting the low wind events at Bancell Road is that the model is probably not predicting escarpment effects well, and that the commonly-used surface similarity theory used in TAPM becomes increasingly invalid as the wind speed becomes low. Under such conditions, it is expected that the model would predict the stack-level ($\sim 100\text{ m}$) wind speeds better than the surface winds.

One possible way to correct for errors in the model winds is to apply a procedure known as “wind data assimilation” which blends the model approximations with the meteorological observations. However, this method is only useful where there are wind observations and no extreme variations in topography. Models applied for forecasting purposes cannot use data assimilation, and the procedure would have been inappropriate in this study. Wind data assimilation will be examined in the Phase 2 TAPM study.

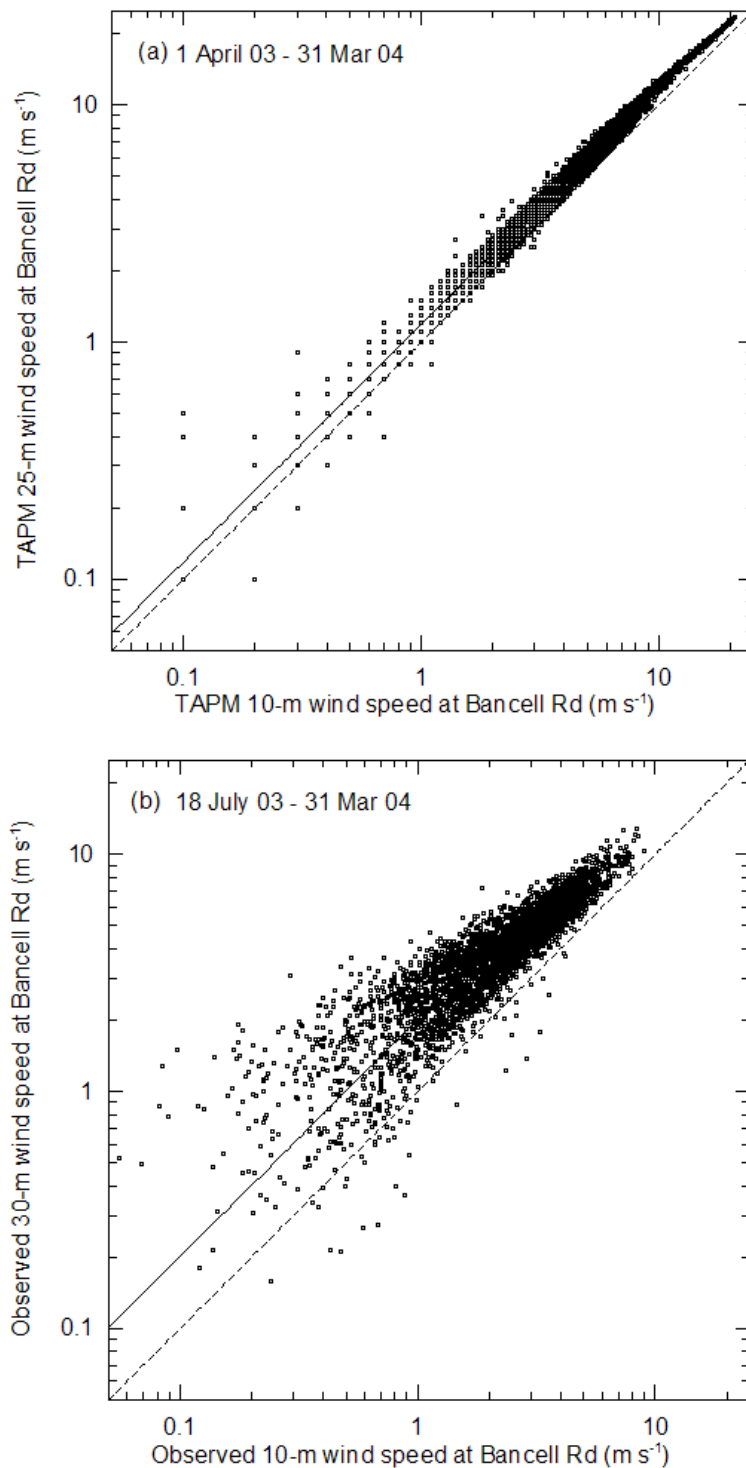


Figure 46: Scatter plots of (a) TAPM 10-m wind speed vs. TAPM 25-m wind speed, and (b) Observed 10-m wind speed vs. observed 30-m wind speed at Bancell Road. In (b) the wind data corresponding to the sector $45^\circ - 145^\circ$ are not included. The solid lines are regression fits for the wind speed range $0.5 - 2 \text{ m s}^{-1}$.

10. Comparison with other modelling studies

Meteorological models have been used in the past by various researchers. Examples of previous quantitative model evaluations include the case studies of Steyn and McKendry (1988) using the Colorado State University (CSU) model for the Vancouver area, Ulrickson and Mass (1990) using the CSU model for the Los Angeles basin, Seaman et al. (1995, 1996) using the MM5 model for Southern California, and Lyons et al. (1995) using the Regional Atmospheric Modeling System (RAMS) for the Lake Michigan region. These studies presented statistics for near-surface monitoring stations which included wind speed (all studies) and temperature (Steyn and McKendry, 1988, only), using selections of the statistical measures described in this report.

Most of the above case studies involved short simulation periods (a few days), but measurements from a large number of monitoring sites were used for model comparison. These studies presented index of agreement (IOA) values for wind speed in the range 0.35–0.75, with an average value of 0.56, and the quality of the simulations from these studies was considered in the reports to be good. None of the RMSE values for winds contained significant systematic bias. For temperature, the average IOA value obtained by Steyn and McKendry (1988) was 0.33. The overall RMSE value was 3.0, which was dominated by the RMSE_S component and so contained significant bias, which also affected the IOA value.

More recently, Physick and Noonan (2000) presented twelve separate case study results using MM5 for Hong Kong, and they obtained IOA values for wind speed in the range 0.36–0.71, with an average value of 0.55.

These results imply that an IOA value greater than 0.5 represents a good result for prediction of meteorology. Table 13 gives index of agreement (IOA) values for other models and well as for TAPM.

Previous TAPM has previously been used to model year-long meteorology and air pollution for the industrial area of Kwinana (Hurley et al., 2001, 2002). In this study, for near-surface meteorology, the average IOA for wind speed was 0.67. In the TAPM simulations used to model year-long urban meteorology, photochemical smog and particulate matter in Melbourne (Hurley et al., 2003a), the IOA ranged between 0.79–0.88 for the 10-m wind speed, 0.81–0.89 for the *U* component, 0.89–0.94 for the *V* component, and 0.93–0.96 for the temperature. The systematic RMSE was smaller than the unsystematic RMSE in these simulations. A comparison of TAPM performance with international model validation data sets for Indianapolis and Kincaid (Luhar and Hurley, 2003) shows that for the near-surface meteorology the IOA was between 0.80–0.86 for wind speed, 0.83–0.88 for the *U* component, 0.87–0.90 for the *V* component, 0.94–0.97 for temperature, and 0.89–0.95 for net radiation. These two case studies showed an overestimation of net radiation by the model, which is also the case in the present study. Table 13 gives IOA values for other TAPM studies.

Table 13: Index of agreement (IOA) values for near-surface meteorology from other modelling studies.

Model	Location	Duration	Variable	IOA	Reference
CSU	Los Angeles Basin (USA)	Two days (44 – 48 sites)	<i>WS</i>	0.35–0.75	Ulrickson and Mass (1990)
CSU	Vancouver	One day (up to 23 sites)	<i>WS</i>	0.41–0.61	Steyn and McKendry (1988)
			<i>T</i>	0.11–0.74	
MM5	Southern California	Two summer cases (120 h each)	<i>WS</i>	0.51, 0.76*	Seaman et al. (1995)
MM5	Los Angeles Basin (USA)	Four days (120 h)	<i>WS</i>	0.55*	Seaman et al. (2000)
MM5	Lake Michigan	Two summer cases (120 h each)	<i>WS</i>	0.54, 0.62*	Seaman et al. (2000), Shafram et al. (2000)
MM5	Hong Kong	12 case studies	<i>WS</i>	0.36–0.71	Physick and Noonan (2000)
RAMS	Lake Michigan	Four summer cases (120 h each)	<i>WS</i>	0.59*	Lyons et al. (1995)
TAPM (v2.0)	Kwinana (WA)	One year (1997), 6 sites	<i>WS</i>	0.67	Hurley et al. (2002)
			<i>U</i>	0.87	
			<i>V</i>	0.84	
			<i>T</i>	0.96	
TAPM (v2.3)	Pilbara (WA)	One year (1999), 2 sites	<i>WS</i>	0.63–0.79	Hurley et al. (2003b)
			<i>U</i>	0.89–0.92	
			<i>V</i>	0.85–0.87	
			<i>T</i>	0.94–0.95	
			<i>R_H</i>	0.87–0.88	
TAPM (v2.0)	Cape Grim (TAS)	Dec. 1997 – Feb. 1998, 1 site, 2 levels	<i>WS</i>	0.71–0.85	Hurley et al. (2002)
			<i>U</i>	0.89–0.94	
			<i>V</i>	0.82–0.89	
			<i>T</i>	0.92	
			<i>R_H</i>	0.70	
TAPM (v2.0)	Melbourne	July 1997 – June 1998, 9 sites	<i>WS</i>	0.79–0.88	Hurley et al. (2003a)
			<i>U</i>	0.81–0.89	
			<i>V</i>	0.89–0.94	
			<i>T</i>	0.93–96	

TAPM (v2.0)	Perth	One year (1999), 3 sites	<i>WS</i> <i>U</i> <i>V</i> <i>T</i>	0.78 0.91 0.90 0.95	Hurley et al. (2002)
TAPM (v2.0)	Kincaid (USA)	16 May – 1 June 1981, 1 site, 2 levels	<i>WS</i> <i>U</i> <i>V</i> <i>T</i> <i>R_n</i>	0.80 0.83 0.87 0.94 0.93	Luhar and Hurley (2003)
TAPM (v2.0)	Indianapolis (USA)	16 Sep.– 12 Oct. 1985, 2 sites	<i>WS</i> <i>U</i> <i>V</i> <i>T</i> <i>R_n</i>	0.86 0.88 0.90 0.97 0.89	Luhar and Hurley (2003)
TAPM (v2.0)	Anglesea (Vic.)	One year (2002), 1 site	<i>WS</i> <i>U</i> <i>V</i> <i>T</i> <i>R_H</i>	0.81 0.84 0.91 0.91 0.73	Hill and Hurley (2003)
TAPM (v2.0)	Kalgoorlie (WA)	One year (2000), 1 site	<i>WS</i> <i>U</i> <i>V</i> <i>T</i>	0.81 0.95 0.92 0.93	Edwards et al. (2004)
TAPM (v2.6)	Wagerup (WA)	One year (Apr 03 – Mar 04), 2 sites	<i>WS</i> <i>U</i> <i>V</i> <i>T</i> <i>R_H</i> <i>R_n</i>	0.65–0.73 0.79–0.83 0.90–0.92 0.97 0.87 0.94	Present study

*With data assimilation

For the model comparison presented in this report for Wagerup, the overall IOA for the near-surface meteorology (with winds at 30 m AGL) at Bancell Road is 0.65 for wind speed, 0.79 for the *U* component, and 0.92 for the *V* component, 0.97 for temperature, 0.94 for net radiation, and 0.87 for relative humidity. For the winter months, when low to moderate winds are important from point of view of point source emissions from the Refinery, the respective IOA values are 0.79, 0.86, 0.93, 0.89, and 0.81. The overall

IOA for the near-surface meteorology at RDA is 0.73 for wind speed, 0.83 for the U component, and 0.90 for the V component. For the summer months, when high and variable winds are relevant from the point of view of dust emissions and management at RDA, the respective IOA values are 0.65, 0.79 and 0.84. In the summer months, the IOA values for net radiation and relative humidity at Bancell Road are 0.94 and 0.90, respectively.

These above comparisons suggest that TAPM's overall performance is as good as and in some cases better than some of the other prognostic meteorological models mentioned above. The performance of TAPM at Wagerup is comparable to its performance elsewhere for the near-surface meteorology, except that TAPM generally predicts stronger wind speeds at Wagerup than the measurements, and its performance for wind speed for Wagerup is not as good as for other locations. It should be noted, however, that all of above studies were performed for different regions, and the performance of a model may be partly dependent on the complexity of the area being studied.

11. Summary and conclusions

The Wagerup Alumina Refinery of Alcoa World Alumina Australia is located about 130 km south of Perth in Western Australia. The work presented in this report is part of a study entitled “Meteorological and Dispersion Modelling Using TAPM (version 2.6) for Wagerup”, addressing three closely defined objectives. This report deals with the first objective (Phase 1: Meteorology), which was to evaluate the capability of CSIRO’s The Air Pollution Model (TAPM) to acceptably produce hourly-averaged meteorological predictions matching available field observations in the close proximity of the Wagerup Refinery. The reports of Phase 2 (Dispersion) and Phase 3 (TAPM modelling for Health Risk Assessment) will be presented subsequently.

TAPM is a prognostic meteorological and air pollution dispersion model developed by CSIRO Atmospheric Research (see <http://www.dar.csiro.au/tapm>). The main advantage of the prognostic approach is that rather than requiring local meteorology it calculates it. The meteorological component of TAPM predicts the local-scale flow, such as sea breezes and terrain-induced circulations, using the larger-scale synoptic meteorology as boundary conditions. The air pollution component uses the model-predicted three-dimensional meteorology and turbulence.

The period April 2003–March 2004 was selected as the period for model evaluation, because it encompasses a complete, continuous winter season and a complete, continuous summer season, with the best meteorological data currently available. No previous continuous seasons were considered because new meteorological measurement systems were deployed in the year 2003 (e.g. a 30-m tower at Bancell Road, and radiosonde releases), providing extra meteorological data for a more comprehensive model evaluation.

The specific components of the Phase 1 objective included:

- Development of a finer, more accurate land-use database for Wagerup for use as input in TAPM than the default database.
- Derivation of the refinery-generated heat flux, its inclusion in TAPM, and evaluation of its effect on meteorological predictions.
- Analysis of the near-surface meteorological data from the Bancell Road and Residue Disposal Area (RDA) monitoring sites.
- Evaluation of TAPM performance against the locally observed meteorology using an internationally accepted set of statistical and graphical methods.
- Comparison the model profiles of wind speed, wind direction, and temperature with the radiosonde data from the 2003 campaign.
- Evaluation of the sensitivity of TAPM to surface roughness and deep soil moisture content.
- An analysis of underlying factors that influence the degree of disagreement in the model vs. observations comparison.
- Comparison of the model evaluation results with other studies.

As part of the Phase 1 work, the default land-use database used as input in TAPM was replaced by a more refined Wagerup specific land-use database at a resolution of 250 m × 250 m using GIS maps and a recent aerial photo covering an area of approximately 25 km × 25 km centred on the Refinery. The Refinery, the RDA and the adjacent cooling lakes were resolved.

An estimation of the Refinery-generated heat flux was made using Alcoa supplied information on heat balance for Wagerup Refinery based on known energy inputs, outputs and losses. The estimated heat flux value of 150 W m⁻² was added to the TAPM surface-energy balance equation.

TAPM was run with four nested grid domains at 20, 7, 2, 0.5 km resolution for meteorology (31 × 31 grid points). The lowest ten of the 25 vertical levels were 10, 25, 50, 100, 150, 200, 250, 300, 400 and 500 m. The default databases of topography, monthly sea-surface temperature, soil types, deep soil moisture content, and deep soil temperature were used. The results from the innermost model grid domain (with a resolution of 0.5 km) were used to compare with the measurements.

The use of the derived Wagerup-specific land use, together with the refinery-generated heat flux, in the model improved the temperature and relative humidity predictions at Bancell Road, but only slightly.

A sensitivity test indicated that increasing or decreasing the deep soil moisture content to acceptable bounds in the model does not improve the agreement between the modelled meteorology and the observations.

A sensitivity test indicates that increasing the roughness length for the area to an acceptable limit in the model does not improve the agreement between the modelled meteorology and the observations.

Scatter plots, probability density function (or frequency) plots, and model evaluation statistics, such as observed and predicted means and standard deviations, correlation coefficient, root mean square error, systematic root mean square error, unsystematic root mean square error and index of agreement, were used to test TAPM's performance. The model evaluation was done for whole year, daytime, nighttime, winter period and summer period.

The meteorological measurements used in the test of TAPM against observations were: hourly-averaged wind speed, wind direction and temperature (all measured at both 10 m and 30 m AGL), net radiation, and relative humidity observations taken at Alcoa's Bancell Road monitoring site; the hourly-averaged wind speed and wind direction observations taken at 8 m AGL at the RDA monitoring site; and the radiosonde profiles of wind speed, wind direction, temperature and relative humidity from five morning releases conducted over a 3-day period in July 2003. Statistics and graphs of these tests are presented in this report.

Some particular inaccuracies in the wind speed, wind direction and net radiation measurements at Wagerup, already identified, will cause discrepancies between the TAPM outputs and meteorological observations at Wagerup. These are reviewed in the report.

The agreement between the TAPM predictions and the measurements, as judged by the index of agreement, for Wagerup is the highest for temperature, followed by net radiation, relative humidity, wind direction and wind speed. The model wind predictions are better in the daytime than in the nighttime, and they are better in winter than in summer. The overall wind-speed comparison at Bancell Road is dominated by the strong nighttime easterlies/south-easterlies. The model performance for wind predictions at RDA is better than that at Bancell Road.

The performance of TAPM in predicting the local meteorology at Wagerup is comparable to its performance in predicting the near-surface meteorology elsewhere in the world. TAPM generally predicts stronger wind speeds at Wagerup, and its performance for wind speed for Wagerup is not as good as for other locations.

TAPM's overall performance in predicting local meteorology at Wagerup is as good as and in some cases better than the available published accounts of three other internationally accepted prognostic meteorological models predicting meteorology at other locations.

The performance of the model is partly dependent on the complexity of the area being studied. The Bancell Road site is only about 1 km west from the western foothills of the north-south Darling escarpment, which rises to about 200 m within a distance of about 1.5 km from the foothills. It is possible that the Bancell Road site is sheltered by the escarpment for the easterly/south-easterly winds, and that the model is not able to simulate properly.

The limitations in TAPM predictions arise from these reasons: approximations to the underlying physics; uncertainties in the input data; problems of matching of the scale of the model to the observations. These are basic limitations that arise from current scientific knowledge and computing power.

References

- AS2923: 1987. Australian Standard: Ambient air – guide for measurement of horizontal wind for air quality applications. Standards Association of Australia, North Sydney, pp. 139–153.
- Edwards, M., Hurley, P., Physick, W.: 2004. Verification of TAPM meteorological predictions using sodar data in the Kalgoorlie region. *Australian Meteorological Magazine* **53**, 29–37.
- EPAV: 2000. AUSPLUME Gaussian Plume Dispersion Model: Technical User Manual. Environment Protection Authority of Victoria, Australia, <http://www.epa.vic.gov.au>.
- Gill, G.C., Olsson, L.E., Sela, J., Suda, M.: 1967. Accuracy of wind measurements on towers or stacks. *Bulletin of the American Meteorological Society* **48**, 665–675.
- Garratt, J.R.: 1994. The Atmospheric Boundary Layer. Cambridge University Press, Cambridge (UK), 316 pp.
- Goodin, W. R., McRae, G.J., Seinfeld, J. H.: 1980. An objective analysis technique for constructing three-dimensional urban-scale wind fields. *Journal of Applied Meteorology* **19**, 98–108.
- Hibberd, M., Physick, B., Park, G.: 2003. Verification of several aspects of TAPM against multi-year monitoring data at Collie. *Proceedings of the 17th International Clean Air and Environment Conference*, 23–27 November 2003, Newcastle, Australia.
- Hill, J., Hurley, P.: 2003. The use of TAPM at Anglesea. *Proceedings of the 17th International Clean Air and Environment Conference*, 23–27 November 2003, Newcastle, Australia.
- Hurley, P.: 2002. The Air Pollution Model (TAPM) Version 2. Part 1: Technical Description. CSIRO Atmospheric Research Technical Paper No. 55. Available at <http://www.dar.csiro.au/TAPM>.
- Hurley, P.J., Blockley, A., Rayner, K.: 2001. Verification of a prognostic meteorological and air pollution model for year-long predictions in the Kwinana region of Western Australia. *Atmospheric Environment* **35**, 1871–1880.
- Hurley, P. J., Physick, W. L., Luhar, A. K.: 2002. The Air Pollution Model (TAPM) Version 2. Part 2: Summary of some verification studies. CSIRO Atmospheric Research Technical Paper No. 57. Available at <http://www.dar.csiro.au/TAPM>.

- Hurley, P., Manins, P., Lee, S., Boyle, R., Ng, Y.L., Dewundege, P.: 2003a. Year-long, hi-resolution, urban airshed modelling: verification of TAPM predictions of smog and particles in Melbourne, Australia. *Atmospheric Environment* **37**, 1899–1910.
- Hurley, P., Physick, W., Cope, M., Borgas, M., Brace, P.: 2003b. An evaluation of TAPM for photochemical smog applications in the Pilbara region of WA. *Proceedings of the 17th International Clean Air and Environment Conference*, 23–27 November 2003, Newcastle, Australia.
- Luhar, A.K., Hurley, P.J.: 2003. Evaluation of TAPM, a prognostic meteorological and air pollution model, using urban and rural point-source data. *Atmospheric Environment* **37**, 2795–2810.
- Luhar, A.K., Rao, K.S.: 1994. Lagrangian stochastic dispersion model simulations of tracer data in nocturnal flows over complex terrain. *Atmospheric Environment* **28**, 3417–3431.
- Lyons, W. A., Tremback, C. J., Pielke R. A.: 1995. Applications of the Regional Atmospheric Modeling System (RAMS) to Provide Input to Photochemical Grid Models for the Lake Michigan Ozone Study (LMOS). *Journal of Applied Meteorology* **34**, 1762–1786.
- Oke, T.: 1987. *Boundary Layer Climates*. Methuen & Co. Ltd., London, 435 pp.
- Physick, W. L., Noonan, J. A.: 2000. Mesoscale modelling with MM5 for the PATH study (pollutants in the atmosphere and their transport over Hong Kong). *Preprints of the 11th Joint Conference on Applications of Air Pollution Meteorology with AWMA*, Long Beach, CA, U.S.A., pp. 90–95.
- Pielke, R.A.:1984. *Mesoscale Meteorological Modelling*. Academic Press, Orlando, 612 pp.
- Pitts, O.: 2004. Wagerup Refinery – June and July 2003 Radio Sonde Data. E-mail to P. Coffey of Alcoa, 11 May 2004, Air Assessments, Western Australia.
- Ratto, C.F., Festa, R., Romeo, C., Frumento, O. A., Galluzzi, M.: 1994. Mass-consistent models for wind fields over complex terrain. *Environmental Software* **9**, 247–268.
- Ross, D.G., Smith, I.N., Manins, P.C., Fox, D.G.:1988. Diagnostic wind field modeling for complex terrain: model development and testing. *Journal of Applied Meteorology* **27**, 785–796.
- Sawford, B.L., Luhar, A.K, Noonan, J.A., Yoon, I.-H, Young, S.A, Physick, W.L, Patterson, G.R, Hacker, J.M, Carras, J.N, Williams, D.J., Blockely, A.: 1996. Shoreline Fumigation at Kwinana: a study to assess, validate and improve DISPMOD. Final report. CSIRO Division of Atmospheric Research, Aspendale, 323 pp.

- Seaman, N.: 2000. Meteorological modelling for air-quality assessments. *Atmospheric Environment* **34**, 2231–2259.
- Seaman, N. L., Stauffer, D. R., Lario-Gibbs, A. M.: 1995. A multi-scale four dimensional data assimilation system applied in the San Joaquin Valley during SARMAP. Part I: modeling design and basic performance. *Journal of Applied Meteorology* **34**, 1739–1761.
- Seaman, N. L., Stauffer, D. R., McNally, D. E., Tanrikulu, S.: 1996. Application of the MM5- FDDA meteorological model to the southern California SCAQS-97 domain: Preliminary test using the SCAQS August 1987 case. *Preprints of the 9th Joint Conference on Applications of Air Pollution Meteorology with AWMA*, Atlanta, Georgia, U.S.A., January 28–February 2, 1996.
- Scire, J., Robe, F., Fernau, M., Insley, E., Yamartino, R.: 1997. A users guide for the CALMET meteorological model (version 5). Earth Tech, Inc., Concord MA.
- Scire, J. S., Strimaitis, D. G., Yamartino, R. J.: 2000. A User's Guide for the CALPUFF Dispersion Model (Version 5). Earth Tech, Inc., Concord, USA.
- Shafran, P.C., Seaman, N.L., Gayno, G.A.: 2000. Evaluation of numerical predictions of boundary layer structure during the Lake Michigan ozone study. *Journal of Applied Meteorology* **39**, 412–426.
- SKM: 2002. Wagerup Refinery Odour Assessment. Final report, Sinclair Knight Merz, February 2002.
- SKM: 2003. Alcoa World Alumina Australia: Wagerup weather station and ambient dust monitoring program review following implementation of audit findings. Sinclair Knight Merz, Bunbury, WA (Australia), 28 June 2004, pp. 27.
- SKM: 2004. Kwinana Refinery Odour Modelling. Final Report to Alcoa, Sinclair Knight Merz, 7 May 2004.
- Steyn, D. G., McKendry, I. G.: 1988. Quantitative and qualitative evaluation of a three-dimensional mesoscale numerical model simulation of a sea breeze in complex terrain. *Monthly Weather Review* **116**, 1914–1926.
- Ulrickson, B. L., Mass, C. F.: 1990. Numerical investigation of mesoscale circulations over the Los Angeles basin. Part I: a verification study, *Monthly Weather Review* **118**, 2138–2161.
- USEPA: 1995. Users guide for the Industrial Source Complex (ISC3) dispersion models. Volume 1 – User instructions, U.S. Environmental Protection Agency, EPA-454/B-95-003a.
- Willmott, C.J.:1981. On the Validation of Models. *Phys. Geography* **2**, 184-194.